Q. J. R. Meteorol. Soc. (1997), **123**, pp. 1227–1282

A physically based scheme for the treatment of stratiform clouds and precipitation in large-scale models. I: Description and evaluation of the microphysical processes

By LEON D. ROTSTAYN*

Commonwealth Scientific and Industrial Research Organization†, Australia

(Received 30 April 1996; revised 5 August 1996)

SUMMARY

A stratiform-cloud and precipitation scheme, incorporating prognostic variables for cloud liquid water and cloud ice, has been developed for the CSIRO global climate model (GCM). The scheme includes physically based treatments of key microphysical processes, turbulent mixing and semi-Lagrangian advection of cloud-water species and interactive cloud radiative properties. Objectives in the development of the scheme were to improve upon the physical realism of parametrizations used in earlier schemes, whilst also trying to provide a scheme with moderate computational overheads.

The parametrized microphysical processes are evaluated in relation to observations and theory, and are compared to treatments used in earlier schemes in a series of short GCM experiments. It is argued that the treatment of precipitation formation in warm, and mixed-phase, stratiform clouds is more realistic in the present scheme than in earlier schemes, which used crude methods for the parametrization of autoconversion, and did not treat key ice-processes in a consistent way. In the present scheme, accretion processes are more important, whereas autoconversion is less important than in earlier schemes.

To determine whether the cloud scheme requires the use of a reduced (split) time-step, the sensitivity of the various terms to the time-step is evaluated in another series of short GCM experiments. It is shown that the various terms are not very sensitive to the time-step, so the scheme can be efficiently implemented without the use of a split time-step. Overall, analytical or time-centred treatments perform better than implicit or explicit schemes, especially in the calculation of the precipitation of cloud ice, where only an accurate analytical treatment is found to perform satisfactorily at large time-steps.

As a preliminary validation of the scheme, zonal-mean fields from a six-year model-run are presented for the month of July. The results generally agree well with observations; in particular, the modelled cloudiness and long-wave cloud-forcing fields are more realistic than those obtained with the standard version of the CSIRO GCM.

KEYWORDS: Clouds Global climate models Microphysics Precipitation

1. INTRODUCTION

Global climate models (GCMs) are the most important tools currently in use for the study of anthropogenically induced climate change, but suffer from large uncertainties in their response to increased levels of greenhouse gases. Cess *et al.* (1990) identified the treatment of clouds as the major cause of the large differences in climate sensitivity found in 19 atmospheric GCMs. Recently, there has been a move towards more physically based treatments of clouds in GCMs and numerical weather prediction (NWP) models (Sundqvist 1978; Le Treut and Li 1988; Sundqvist *et al.* 1989; Smith 1990; Roeckner *et al.* 1992; Ose 1993; Ricard and Royer 1993; Tiedtke 1993; Le Treut *et al.* 1994; Boucher *et al.* 1995; Fowler *et al.* 1996). Most of these schemes have incorporated one or more prognostic cloud-variables, since the traditional approach, in which clouds are diagnosed as a function of relative humidity and other model variables, does not allow the clouds to be fully integrated into the model's hydrological cycle, and provides limited opportunity to improve the physical realism of the modelled clouds. The use of prognostic cloud-schemes is not a panacea, since there is considerable uncertainty about how to treat a number of key processes, and validation of cloud schemes remains a problem, despite the increased availability of satellite observations. Prognostic schemes also have the potential to consume larger amounts of computer time than simple diagnostic schemes; this can be a serious

* Corresponding address: CSIRO Division of Atmospheric Research, Private Mail Bag 1, Aspendale Vic 3195, Australia. e-mail ldr@dar.csiro.au.

† Also Cooperative Research Centre for Southern Hemisphere Meteorology.

problem for climate studies which require lengthy integrations and for NWP where limited time is available to complete a forecast.

The treatment of cloud microphysical processes in earlier prognostic schemes was generally very simple (Sundqvist 1978; Le Treut and Li 1988). Later schemes (Sundqvist *et al.* 1989; Smith 1990; Roeckner *et al.* 1992; Ose 1993; Ricard and Royer 1993; Tiedtke 1993; Le Treut *et al.* 1994) employed more complex, though still highly idealized parametrizations. Although these schemes included some treatment of the microphysics of both warm and cold clouds, the formation of rainfall, for example, was based on intuition. More recent schemes (Boucher *et al.* 1995; Fowler *et al.* 1996) have included more physically-based parametrizations, similar to bulk parametrizations that have been in use for some years in the mesoscale-cloud-modelling community (Tripoli and Cotton 1980; Cotton *et al.* 1982, 1986; Lin *et al.* 1983; Rutledge and Hobbs 1983). These parametrizations are based on concepts—such as observationally based raindrop- (and snowflake-) size distributions, the continuous-collection equation for the accretion of cloud liquid water by falling raindrops (or snowflakes), and the equations which describe the diffusional growth or decay of raindrops or ice particles—that have been developed over several decades by cloud physicists (e.g. Rogers and Yau (1988) hereafter RY88), so they should be more physically realistic than the simple approaches used previously in large-scale models. However, there are large differences between the spatial and temporal scales treated by global models and those treated by mesoscale models; the small time-steps and degree of complexity employed by the microphysics schemes used in mesoscale models render them computationally too expensive for use in extended GCM simulations on current supercomputers. With this in mind, Ghan and Easter (1992) evaluated approximations to the Colorado State University (CSU) cloud-microphysics scheme (Tripoli and Cotton 1980; Cotton *et al.* 1982, 1986) that would permit a tenfold increase in the allowable time-step from a few tens of seconds to a few minutes. Fowler *et al.* (1996) implemented a complex microphysics scheme, based largely on Lin *et al.* (1983) and Rutledge and Hobbs (1983), in the CSU GCM, using a time-splitting approach with a 2 minute time-step in the microphysics scheme. This time-step is small compared to those used for the physics in most global models (typically 10 to 60 minutes) and could be expected to result in a large overhead that might be considered unacceptable in NWP models or in GCMs that are to be used in long integrations. Indeed, Fowler *et al.* (1996) found that inclusion of their cloud-microphysics scheme resulted in a doubling of the computer time required to run the CSU GCM. Boucher *et al.* (1995) included physically based parametrizations of warm-cloud precipitation processes in the Laboratoire de Météorologie Dynamique (LMD), using a time-splitting approach with a 6 minute time-step. Authors of the earlier schemes made no mention of time-splitting, so it seems reasonable to assume that they have used the usual physics time-step of their model for the cloud microphysics. Despite the large range of time-steps implied by this discussion, the sensitivity of the simulated processes to the time-step was not investigated in any of the studies mentioned above, other than by Ghan and Easter (1992) in the context of single-column tests. Also, both Fowler *et al.* (1996) and Boucher *et al.* (1995) treated rainfall as a prognostic quantity, in contrast to earlier schemes, which treated it as a diagnostic quantity that was assumed to fall through the atmosphere in a single time-step. Fowler *et al.* (1996) stated that a time-split prognostic treatment of rainfall is "by far the simplest and most rigorous" approach, but provided no concrete results to support their assertion. The treatment of rain as a diagnostic quantity was one of the approximations evaluated and found to be satisfactory by Ghan and Easter (1992).

The philosophy underlying the approach described here is to attempt to capture the 'essential' physics, without resorting to a highly complex scheme which is difficult to

understand and could have unforeseen effects in the model. It continues the recent trend towards treatments of microphysical processes which are more physically based, but is less complex (in terms of the number of processes treated) than the scheme of Fowler *et al.* (1996). It adds two prognostic variables (cloud liquid water and cloud ice) to the GCM used by the Australian Commonwealth Scientific and Industrial Organization (CSIRO), but, in contrast to the schemes of Boucher *et al.* (1995) and Fowler *et al.* (1996), rain is treated as a diagnostic quantity. Key objectives were to provide for the CSIRO GCM a cloud scheme which was more physically realistic than earlier prognostic schemes, and which also produced cloudiness and cloud radiative-forcing fields which were in better overall agreement with observations than those produced by the model's standard diagnostic cloud-scheme. At the same time, it was considered essential that this should be achieved with an 'acceptable' level of computational overheads. With this in mind, considerable effort was put into an evaluation of the sensitivity of the simulated microphysical processes to the choice of time-step, since the use of a reduced (split) time-step for the microphysical processes would obviously result in additional computational overheads. The present paper shows that the simulated processes are not very sensitive to the time-step; on this basis, it was decided not to use a split time-step for the cloud microphysics. This was a key factor in the implementation of the scheme with moderate computational overheads (see section 7 for details).

An outline of the remainder of the present paper is as follows. Section 2 contains an overview of the CSIRO atmospheric GCM which is used in this study. Section 3 contains a brief description of the cloud scheme, including the treatment of cloud-radiative properties. Section 4 contains a more detailed description and evaluation of the rainfall processes in the scheme, including sensitivity of the processes to the time-step and comparison of the parametrizations with others that have been used in GCMs. Section 5 contains a similar analysis for the frozen precipitation (snow) processes in the scheme. In section 6, zonal-mean results from a six-year run of the model are compared with observations as a preliminary validation of the scheme—a more detailed validation of the large-scale fields produced by the scheme will be given in a subsequent paper (Part II). Section 7 contains a summary and concluding discussion. All quantities referred to in the text have SI units, except where it is explicitly stated otherwise.

2. Overview of the CSIRO atmospheric GCM

The CSIRO atmospheric GCM is a spectral model which utilizes the flux form (Gordon 1981) of the primitive equations; an earlier version (Mark 1) has been described in detail by McGregor *et al.* (1993). Mark 1 had nine vertical levels and horizontal spectral resolution of R21, corresponding to a grid of 56 latitudes and 64 longitudes. The current version (Mark 2) of the CSIRO GCM differs from the earlier Mark 1 in several major respects. It has:

- Variable horizontal resolution, so that the model can be run with spectral resolution of R21, R42 or T63. The use of nine vertical levels has been retained in the standard Mark 2 version of the model. The experiments described in the present paper were run at R21, but with 18 levels, in order to achieve a better representation of physical processes in the vertical. The 18-level R21 version requires a time-step of 24 minutes; the leapfrog scheme in the model means that the time-step effectively 'seen' by the physical parametrizations is 48 minutes. The 18 levels are at $\sigma = 0.9955$, 0.9784, 0.9458, 0.8999, 0.8426, 0.7761, 0.7023, 0.6235, 0.5415, 0.4585, 0.3765, 0.2977, 0.2239, 0.1574, 0.1001, 0.0542, 0.0216 and 0.0045 where $\sigma = p/p_*$ is the model's vertical coordinate, p is pressure and p_* is surface pressure.

• A new soil-canopy scheme (Kowalczyk *et al.* 1991) which includes spatially varying data-sets of soil type, albedo, roughness length, canopy resistance and dominant vegetation-type. Physical processes parametrized by the scheme include canopy interception of moisture, runoff (including deep soil percolation) and snow accumulation and melting.

• A semi-Lagrangian scheme for moisture advection, instead of the pseudo-spectral scheme used in Mark 1. The semi-Lagrangian scheme includes an economical scheme for the calculation of the departure points of the trajectories (McGregor 1993) and uses cubic Lagrangian interpolation to calculate the field values at the departure points. A quasi-monotone scheme (Bermejo and Staniforth 1992) is used in the vertical-advection routine to prevent the generation of spurious oscillations and ensure non-negativity of the interpolated moisture values. Any negative values generated by the horizontal-interpolation procedure are simply truncated to zero. Conservation of total global moisture is enforced by an a posteriori adjustment to the increments of the water-vapour mixing ratio.

• A new sea-ice scheme, based on the dynamical model of Flato and Hibler (1990) and the thermodynamic model of Semtner (1976). The new scheme allows the fraction of leads (open water) to vary with the prevailing winds and ocean currents, and allows calculation of the surface fluxes of heat, moisture and momentum through the leads, whereas the simple thermodynamic model that was used in Mark 1 assumed that sea-ice points were totally covered with ice.

• Minor changes to the model dynamics: inclusion of a modified thermodynamic variable (Simmons and Jiabin 1991) which reduces noise in the surface pressure field that had become apparent at the higher horizontal resolutions, and an implicit treatment of the vorticity equation (Simmons *et al.* 1989), adapted to the flux form of the equations used by the CSIRO GCM.

Other physical parametrizations in the model include:

• A radiation scheme based on Schwarzkopf and Fels (1991) for the long wave and Lacis and Hansen (1974) for the short wave. The radiation scheme includes absorption by water vapour, carbon dioxide and ozone, and Rayleigh scattering of short-wave radiation, but does not include absorption by trace gases or scattering by aerosols. There are three layers of diagnostic clouds, loosely following Slingo (1987). The cloud radiative properties are fixed, with short-wave reflectivity and absorptivity specified as a function of height, and emissivity set to 1.

• A moist convective adjustment (MCA) scheme which generates a mass flux, based on the ideas of Arakawa (1972). Katzfey (1994) compared this scheme with the Betts–Miller, Kuo and Arakawa–Schubert schemes in simulations of an Australian east-coast low using a limited-area model, and found that the performance of the MCA scheme was comparable to that of the Arakawa–Schubert scheme, and superior to that of the Betts–Miller and Kuo schemes.

• Treatment of large-scale precipitation by removal of supersaturation. Evaporation of falling rain is included.

• A turbulent-mixing scheme based on stability-dependent K-theory. The diffusion coefficients for vertical turbulent mixing of heat, momentum and moisture are specified as functions of the Richardson number following Louis (1979). The calculation of the Richardson number includes virtual-temperature effects but not the effect of liquid water.

• Treatment of shallow convection following either Geleyn (1987) or Tiedtke (1988), a version of the latter scheme having been adopted for this study. In this approach, shallow convection is assumed to occur when the lifting condensation-level (LCL) for near-surface air is lower than $\sigma = 0.9$. When this criterion is satisfied, the diffusion coefficients in the turbulent-mixing scheme are increased by 6 $m^2 s^{-1}$ between the LCL and cloud top, and

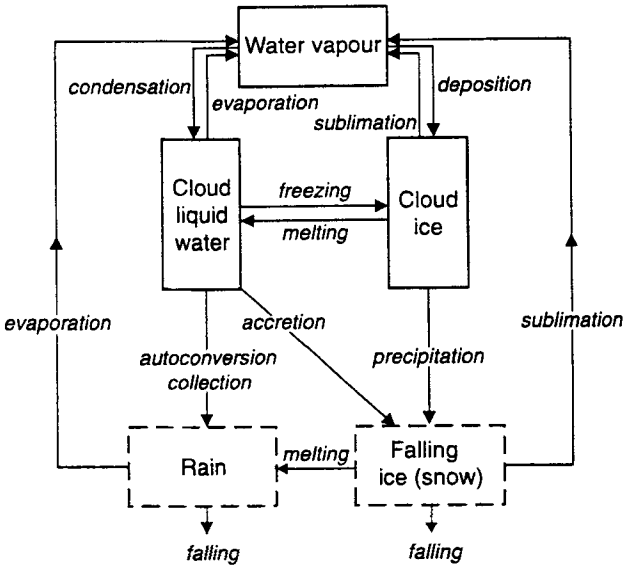

Figure 1. Schematic overview of the microphysical processes treated in the cloud scheme.

by 2 m^2s^{-1} at cloud top. Cloud top is assumed to occur at the level at which near-surface air becomes neutrally buoyant, or at the layer interface closest to $\sigma = 0.75$, whichever is lower.

3. Brief description of the cloud scheme

(a) *Sources and sinks of cloud water*

The new cloud-scheme replaces the diagnostic cloud-scheme and treatment of large-scale precipitation in the standard Mark 2 version of the CSIRO GCM (described above). It incorporates prognostic variables for the cloud-liquid-water mixing ratio (q_l) and the cloud-ice mixing ratio (q_i). The prognostic equations governing the evolution of the new variables may be written as

$$\frac{\partial q_l}{\partial t} = (\dot{q}_l)_{C/E} + (\dot{q}_l)_{F/M} + (\dot{q}_l)_P + (\dot{q}_l)_{AV} + (\dot{q}_l)_{TM} + (\dot{q}_l)_{CV} \tag{1}$$

and

$$\frac{\partial q_i}{\partial t} = (\dot{q}_i)_{CE} + (\dot{q}_i)_{F/M} + (\dot{q}_i)_P + (\dot{q}_i)_{AV} + (\dot{q}_i)_{TM} + (\dot{q}_i)_{CV} \tag{2}$$

respectively. Here, C/E denotes formation or dissipation of stratiform cloud due to condensation or evaporation, F/M denotes freezing or melting, P denotes formation of precipitation, AV denotes advection by the large-scale flow, TM denotes vertical turbulent mixing and CV denotes convection. The convection term is not yet implemented, as the convection scheme in the model does not detrain cloud liquid water or cloud ice. However, a simple diagnostic treatment of convective cloudiness is included, as described below.

Figure 1 contains a schematic overview of the microphysical processes included in the scheme. Processes not shown are advection and turbulent mixing, which transfer cloud liquid water and cloud ice between grid boxes, but do not result in conversion among

the variables within a grid box. For simplicity, a single variable is used to represent all forms of falling ice, so that no distinction is made between falling ice-crystals, snowflakes (aggregates of ice crystals) and graupel (heavily rimed ice-particles). Rain and falling ice are not prognostic variables of the scheme—they are diagnostic quantities which are not carried from one time-step to the next. Rain (with fall speeds of 4–5 m s^{-1}) is assumed to leave the atmosphere in a single time-step. This assumption is difficult to justify for ice, which falls at less than 1 m s^{-1} in the scheme, so ice which enters a grid box from above is permitted to act as a source term for cloud ice. Precipitation of cloud liquid water in the scheme occurs as the result of three processes, i.e.

$$(\dot{q}_l)_P = (\dot{q}_l)_{AC} + (\dot{q}_l)_{AU} + (\dot{q}_l)_{CO}, \tag{3}$$

where AC denotes accretion by falling ice, AU denotes autoconversion (i.e. collision and coalescence of cloud droplets) and CO denotes collection by falling rain. Accretion is a source term for falling ice, whereas autoconversion and collection are source terms for rain (see Fig. 1). Precipitation of cloud ice is treated differently, because of the different physical processes occurring in ice clouds. Ice-forming nuclei (IFN) are relatively rare in the atmosphere (RY88), so ice clouds consist of relatively small numbers of ice crystals many of which grow quickly by diffusion to sufficient size to acquire appreciable fall-speeds. The rate of precipitation of cloud ice is therefore calculated by the use of an observationally based fall-speed. The processes shown in Fig. 1 are treated by three subroutines: the first calculates the formation or dissipation of cloud and the freezing or melting of cloud water, the second calculates frozen precipitation, including sublimation and melting of falling ice and accretion of cloud liquid water by falling ice, and the third calculates the formation of rain by autoconversion and collection by raindrops, and the evaporation of falling rain. The treatment of precipitation is described in detail in sections 4 and 5, whereas the other components of the scheme are described in the remainder of this section.

(*b*) *Formation and dissipation of stratiform cloud*

The formation and dissipation of stratiform cloud is treated by a simple statistical condensation scheme (Smith 1990, hereafter referred to as S90) which uses an assumed triangular probability-density function (PDF) for the sub-grid distribution of the moisture about its grid-box-mean value. S90 expressed the PDF in terms of sub-grid fluctuations of a 'generalized cloud-water' variable

$$Q_c = a_L\{q_t - q_s(T_L, p)\}, \tag{4}$$

which represents the cloud-water mixing ratio* when positive, or the amount of subsaturation when negative. Here, $q_t = q_v + q_l + q_i$ is the total-water mixing ratio and $T_L = T - (L_V/c_p)q_l - (L_S/c_p)q_i$ is the liquid-frozen water temperature (i.e. the temperature that would be obtained by evaporation of all the ice and liquid water in the grid box). The factor

$$a_L = \left\{1 + \frac{L}{c_p}\left(\frac{\partial q_s}{\partial T}\right)_{T_L}\right\}^{-1} \tag{5}$$

accounts for latent heating which increases the temperature inside the cloud above T_L; $\partial q_s/\partial T$ is obtained from the Clausius–Clapeyron equation; $L = L_V$ when $T < 0\,^\circ$C, and $L = L_S$ otherwise.

* Strictly, S90 described his scheme in terms of specific humidities, whereas the present scheme uses mixing ratios, to be consistent with the treatment of water vapour in the CSIRO GCM. The only difference is in the formula used to relate e_s to q_s.

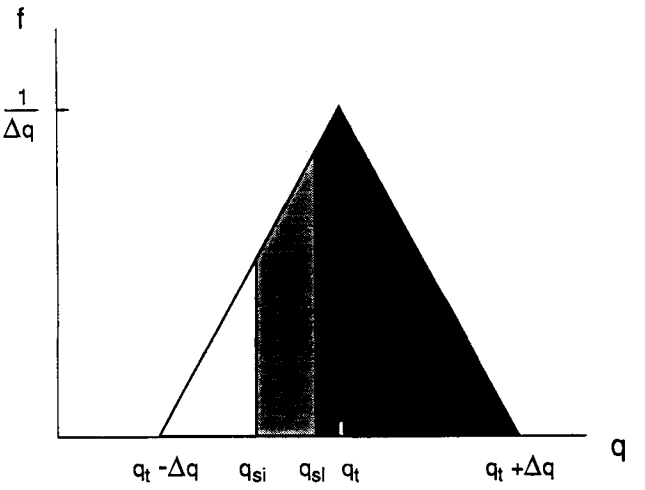

Figure 2. The triangular probability density function $f(q)$ used by the condensation scheme. The distinction between q_{si} and q_{sl} is significant at temperatures between −30 °C and 0 °C, when liquid water and ice can coexist in the heavily shaded region, while only ice can exist in the lightly shaded region. (See discussion in text.)

A mathematically identical but physically simpler formulation is obtained by expressing the PDF $f(q)$ in terms of the sub-grid variation of q_t, while assuming that T_L does not vary within a grid box. In this formulation, the total-water mixing ratio at a point within a grid box (denoted by q, to distinguish it from the grid-box-mean value q_t) is assumed to vary between $q_t - \Delta q$ and $q_t + \Delta q$ as shown in Fig. 2, and cloud is assumed to form in the portion of the grid box which is supersaturated, i.e. the shaded part in Fig. 2. (The two types of shading in Fig. 2 denote regions that are supersaturated with respect to ice ($q > q_{si}$) and liquid water ($q > q_{sl}$) respectively in mixed-phase clouds—the significance of these regions is explained below.) The stratiform cloud fraction is given by

$$C = \int_{q_s}^{\infty} f(q)\,\mathrm{d}q \tag{6}$$

where $q_s = q_{si}$ if $T < 0\,^{\circ}\mathrm{C}$ and $q_s = q_{sl}$ otherwise. The cloud-water mixing ratio $q_c = q_l + q_i$ is calculated on the assumption that sufficient condensation occurs to remove any supersaturation, i.e.

$$q_c = \int_{q_s}^{\infty} a_L\{q - q_s(T_L, p)\} f(q)\,\mathrm{d}q. \tag{7}$$

This assumption is reasonable for liquid-water clouds (in which supersaturations are generally small) but is more difficult to justify for ice clouds, in which air can be significantly supersaturated with respect to ice (Heymsfield and Miloshevich 1995). S90 expressed the width of the PDF in terms of σ_s, the standard deviation of the sub-grid fluctuations of the variable Q_c, and parametrized σ_s as a function of an arbitrary critical relative humidity $\mathrm{RH_{CR}}$ at which clouds begin to form. In the present scheme, the half-width Δq of the triangular distribution $f(q)$ is given by

$$\Delta q = q_s(1 - \mathrm{RH_{CR}}) \tag{8}$$

and is related to the variable σ_s defined by S90 as $\Delta q = \sqrt{6}\sigma_s/a_L$. With this formulation, the present scheme is mathematically identical to the S90 scheme—the equations required

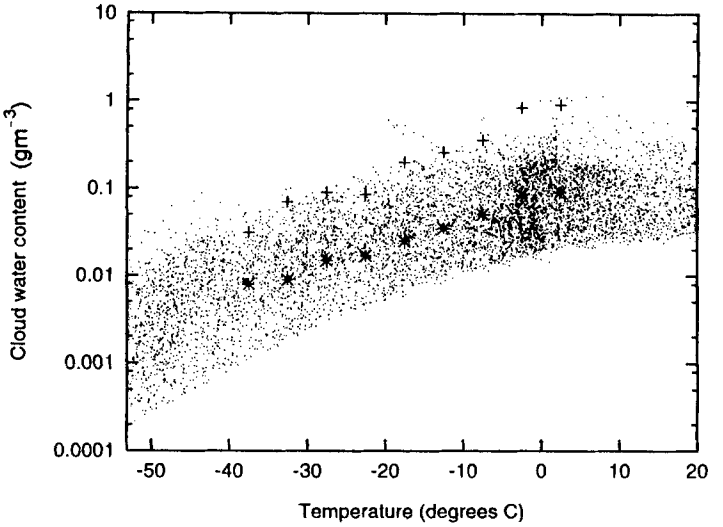

Figure 3. Scatter plot from a single time-step showing the in-cloud water content in stratiform clouds as a function of temperature, together with the median values (shown as asterisks) and 95 percentile values (shown as crosses) of a large number of observations collected by Mazin (1994).

to calculate C and q_c are given in appendix C of S90. The only difference is the simpler physical picture, which clarifies the treatment of mixed-phase clouds described below. In the present scheme, the critical relative humidity RH_{CR} is set to 0.8 at land points and 0.85 at non-land points—this is a crude way to allow for greater sub-grid variability at land points. The modelled cloud-water contents show realistic variation with temperature, as shown in Fig. 3 where the cloud water contents from a single model time-step are plotted along with the median and 95 percentile values of a large number of observations collected by Mazin (1994). Both in the model and in nature, the variation of cloud water content with temperature is primarily due to the increase of $\partial q_s/\partial T$ with temperature.

(c) *Freezing of cloud liquid water and melting of cloud ice*

Freezing of cloud liquid water is assumed to occur instantaneously at temperatures less than $-30°C$, while melting of cloud ice occurs instantaneously at temperatures greater than $0°C$. Between these two temperatures, liquid water and ice are allowed to coexist in the model, so an approach is needed to determine the fraction of cloud water that is liquid. This is difficult to treat realistically in large-scale models, since the physical processes involved in mixed-phase clouds are very complex and not completely understood (RY88). Ideally, the treatment adopted should be able to simulate the life cycle of real mixed-phase clouds, which consist mainly of liquid water initially (because of the relative abundance of cloud condensation nuclei (CCN) compared to IFN), but contain increasing amounts of ice as they evolve, since ice crystals grow at the expense of liquid water as a result of the difference between the saturation vapour pressures with respect to ice and liquid water (often referred to as the Bergeron–Findeisen mechanism). It is also desirable that the treatment should ensure that, at a given temperature, deep clouds (represented by multilayer clouds in the model) are more likely to be glaciated than thin clouds (Ryan 1996), since the lower levels of deep clouds are 'seeded' by ice falling from above. This 'seeder-feeder' mechanism is thought to be responsible for most of the precipitation produced by mid-latitude stratiform clouds (e.g. Rutledge and Hobbs (1983), hereafter RH83).

Most schemes used in GCMs (S90; Ose 1993; Tiedtke 1993; Kristjánsson 1994; Boucher *et al.* 1995) have used some form of interpolation to specify the liquid fraction at temperatures below freezing, although the form of the interpolation and the lower limit (at which all cloud water is assumed frozen) differ between schemes. For example, S90 used a quadratic function of temperature to specify the liquid fraction at temperatures between 0 °C and −15 °C, while Ose (1993) used linear interpolation between −5 °C and −40 °C for stratiform cloud. Although cloud liquid water has been observed at temperatures as low as −40 °C (Heymsfield 1993), Ryan (1996) has argued, based on a review of a wide range of observations of stratiform clouds, that at temperatures below −15 °C and away from regions of embedded convection, the incidence of liquid water is low. This suggests that stratiform clouds in large-scale models should contain relatively little liquid water at temperatures below −15 °C, provided that a separate treatment of convective clouds is included to represent the embedded convection. The interpolation approach, while simple to implement, has a number of drawbacks. For example, ice falling into a sub-freezing model-layer can be forced to 'melt' in order to achieve the prescribed fraction of the liquid at that temperature. Also, the interpolation approach does not model the glaciation of deep clouds realistically. The alternative approach of explicitly parametrizing the processes that result in glaciation of clouds is appealing, but suffers from various uncertainties, especially (but not exclusively) on the spatial and temporal scales resolved by current GCMs. An approach of this type is outlined in appendix A, along with a brief discussion of some of the difficulties.

In view of these difficulties, the following relatively simple approach is adopted here for the treatment of mixed-phase clouds (i.e. clouds at temperatures between −30 °C and 0 °C).

1. The cloud fraction C and the total-cloud-water mixing ratio q_c are calculated, following S90 and using $q_s = q_{si}$ in (6) and (7). This calculation implies that cloud can exist in the portion of the grid box that is supersaturated with respect to ice (i.e. in the shaded area in Fig. 2), and that sufficient condensation occurs to remove any supersaturation with respect to ice.

2. The updated-cloud-liquid water mixing ratio q_l is calculated using (7), but with $q_s = q_{sl}$; i.e. it is assumed that supercooled liquid water can coexist with ice in the part of the grid box which is supersaturated with respect to liquid water (i.e. in the heavily shaded area in Fig. 2), while only ice can exist in the part of the cloud that is subsaturated with respect to liquid water (i.e. in the lightly shaded area in Fig. 2). This is the maximum amount of liquid water that can exist under the assumed PDF.

3. The updated cloud-ice mixing ratio q_i is calculated as the difference between the total-cloud-water mixing ratio and the liquid-water mixing ratio, i.e. $q_i = q_c - q_l$.

4. Since ice should not spuriously melt at sub-freezing temperatures, a further condition is imposed. The updated q_i is adjusted so that it is not less than its value before the condensation calculation, unless the total amount of condensate is found to decrease, when q_i is permitted to decrease through sublimation, in proportion to the decrease in the total amount of condensate. If this condition is invoked, the updated q_l is also adjusted so that the total cloud water q_c remains consistent with that calculated previously.

Though simple, this calculation does contain some of the key physics described in appendix A: it is driven by the relative difference between the saturation mixing ratios with respect to ice and liquid water, by the amount of ice pre-existing in the cloud, and also by the total amount of condensate. The last factor enters the calculation because, in a very moist area, a large fraction of the grid box may exceed saturation with respect to liquid water, while in a less moist area some ice cloud may form when no part of the grid box

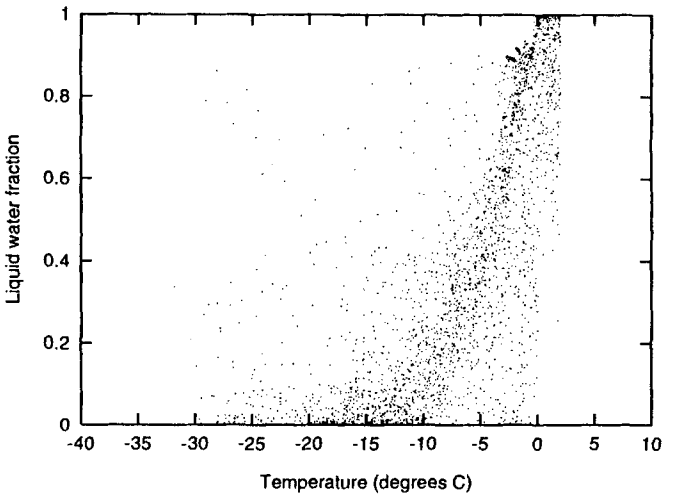

Figure 4. Scatter plot from a single time-step showing the liquid-water fraction in stratiform clouds as a function of temperature. Only points with stratiform-cloud fraction greater than 0.2 are shown, so as not to bias the results by the inclusion of points with very low cloud-water contents.

is saturated with respect to liquid water (see Fig. 2). The relative difference $(q_{sl} - q_{si})/q_{si}$ decreases monotonically with decreasing temperature and is the key parameter driving the calculation described above. It behaves differently from the absolute difference $q_{sl} - q_{si}$, which reaches a maximum around $-12\,^{\circ}C$. Figure 2 shows that it is the relative (rather than the absolute) difference which drives the above calculation, since the relevant quantity is the ratio of $q_{sl} - q_{si}$ to the half-width Δq, where Δq is a linear function of q_{si} given by (8). This relative difference also appears as a key parameter in the physically based treatment discussed in appendix A.

Freezing of cloud liquid water can also occur by riming, the accretion of liquid water by ice which falls from above into a grid box containing supercooled liquid water, thus representing the increased likelihood of glaciation in deep clouds (see section 5). Freezing of cloud liquid water through deposition on ice falling from above has been omitted from the present scheme, as it is unclear how to parametrize this process in a manner which is consistent with the treatment of mixed-phase clouds just described (see appendix A). The liquid-water fractions generated by the scheme during a single time-step are plotted against temperature in Fig. 4, and may be compared with observations made by the Meteorological Research Flight in frontal and other stratiform clouds (see Fig. 5 which is reproduced from Ryan (1996) by permission of the American Meteorological Society). The liquid-water fractions generated by the scheme look realistic when compared with the observations, especially in view of the uncertainty in the observed data, although the modelled liquid-water fractions tend to be somewhat higher than those observed at higher temperatures. Note also that the scheme contains no mechanism which might generate larger liquid-water fractions in continental clouds than in maritime clouds, which the observations suggest; this is thought to be related to the broader droplet-size distributions found in maritime clouds, but the mechanism is uncertain (Rangno and Hobbs 1994). However, the fairly realistic variation of liquid-water fraction with temperature shown in Fig. 4 suggests that, in the mean, the relative difference between q_{si} and q_{sl} is the single most important factor which determines the liquid-water fraction in real clouds. The observations in Fig. 5 may also be compared with those shown for frontal clouds alone by Bower *et al.* (1996); the

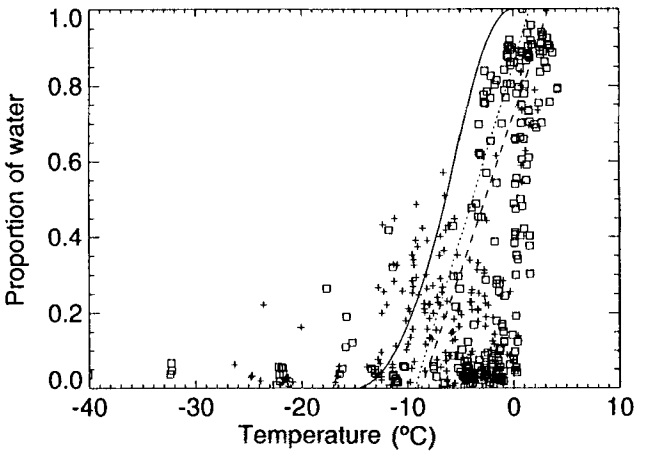

Figure 5. Plot of aircraft observations of the proportion of liquid water as a function of temperature in stratiform clouds. Crosses indicate clouds in continental airmasses and squares indicate clouds in maritime airmasses. Reproduced by permission of the American Meteorological Society.

points with low liquid-water fractions at relatively high temperatures correspond mainly with the deep frontal clouds, rather than shallower clouds such as stratocumulus.

(*d*) *Other sources and sinks of cloud water*

Advection of the cloud-water variables q_l and q_i is handled by the semi-Lagrangian scheme that is used for advection of the water-vapour mixing ratio q_v in the standard version of the model (described above). For the cloud-water variables, the quasi-monotone scheme of Bermejo and Staniforth (1992) is applied to both the vertical and horizontal advection, thereby suppressing the generation of negative values or spurious oscillations in regions of sharp gradients. The advection of cloud water makes only a slight difference to the modelled cloud-fields (consistent with the findings of others, such as Fowler *et al.* (1996)). It is retained, however, for completeness and in the expectation that, when a more realistic treatment of anvil cirrus is included, the advection term will become more important, since anvil cirrus clouds have long lifetimes and can be advected over large distances (Randall 1989).

Vertical turbulent mixing of cloud liquid water and cloud ice is implemented along similar lines to the model's usual turbulent-mixing scheme. The inclusion of vertical mixing of the cloud-water species results in a slight decrease in low cloud and a slight increase in middle-level cloud. Also included is a modification to the Richardson number which accounts for the latent heating and cloud-water loading in cloudy air, similar to that described by S90. The overall effect of the modified Richardson number is to slightly increase the instability of cloudy layers, as the destabilizing effect of the latent heating tends to outweigh the stabilizing effect of the cloud-water loading. This results in a more vigorous hydrological cycle with less low-cloud cover and slightly more middle-level cloud.

(*e*) *Diagnostic treatment of convective clouds*

A simple diagnostic treatment of convective cloudiness, similar to the Slingo (1987) scheme used in the standard Mark 2 version of the CSIRO GCM, has been retained for

now. Following Hack *et al.* (1993), the cover of cenvective cloud is set to

$$\widetilde{C_{CV}} = a_{CV} + b_{CV} \ln(1 + R_{CV}) \tag{9}$$

where R_{CV} is the convective rainfall rate at cloud base and a_{CV} and b_{CV} are tunable constants (currently set to 0.2 and 0.07 respectively, with R_{CV} in mm d^{-1}). With this formulation, a_{CV} is the convective cloud cover for non-precipitating (shallow) convection. The convective cloud is then assumed to be randomly overlapped, so that the fraction of convective cloud at each model level within the convectively active region is given by

$$C_{CV} = 1 - (1 - \widetilde{C_{CV}})^{1/N_{CV}} \tag{10}$$

where N_{CV} is the number of convectively active levels. The water content of convective clouds is specified as 0.2 g m^{-3}, based on observations given by Gayet *et al.* (1993). This water content is assumed to be in the form of liquid water at temperatures above 0 °C and in the form of ice at temperatures below −35 °C. Between 0 °C and −35 °C, the fraction occurring as liquid water is specified by linear interpolation in temperature. When convective cloud is diagnosed in a grid box, the stratiform condensation-scheme is applied only in the environmental air outside the convective cloud. This avoids 'double counting' of cloud when convective and stratiform cloud coexist in a grid box. A total cloud-amount consisting of the sum of the convective and stratiform cloud amounts, with cloud-water content given by the weighted mean of the convective and stratiform values, is then computed for input to the model's radiation scheme.

(*f*) *Cloud radiative properties*

The radiation scheme in the CSIRO GCM assumes random overlap between cloud layers and requires the specification of the bulk cloud radiative properties, i.e. the short-wave reflectivity and absorptivity and the broadband long-wave emissivity. In the standard version of the model, the radiative properties of clouds are prescribed, varying as a function of height only. In the version with prognostic cloud-water, the short-wave properties are calculated for warm clouds following Slingo (1989) and using a similar scheme for ice clouds (Francis *et al.* 1994). Both schemes use the delta–Eddington approximation to calculate the short-wave properties for four bands, which are then averaged to give the properties for the two bands used by the model's short-wave radiation scheme. Both schemes require as input parameters the liquid- (or ice-) water path and the effective radius r_e. The liquid- and ice-water paths are provided by the cloud scheme—the values passed to the radiation scheme are taken as averages of those generated by the cloud scheme before and after the calculation of precipitation, and are also averaged over several time-steps, since the radiation scheme is called just once every two model hours. For warm clouds, r_e is specified as a function of liquid-water content and droplet concentration following Martin *et al.* (1994), with a prescribed droplet-concentration of 1×10^8 m^{-3} for maritime clouds and 5×10^8 m^{-3} for continental clouds. For simplicity, continental clouds are taken to be those at land grid-points and maritime clouds are taken to be those at non-land grid-points. As in the study by Jones *et al.* (1994), the liquid-water content at cloud top is used in the calculation of r_e. For ice clouds, r_e is diagnosed from a relation between ice content W_i and visible volume extinction coefficient β_{ext} deduced from observations by Platt (1994), viz.

$$\beta_{ext} = 0.032 W_i^{0.333} \tag{11}$$

if β_{ext} and W_i are both given in SI units (m^{-1} and kg m^{-3} respectively). Equation (11) was derived on the basis that ice crystals can be approximated as spheres—a more sophisticated

parametrization, which accounts for ice-crystal morphology, is given by Platt (1997). Since $r_e = 3W_i/(2\rho_i\beta_{ext})$, (11) implies that the effective radius increases with W_i according to

$$r_e = 0.051 W_i^{0.667} \tag{12}$$

in contrast to many current schemes which specify a fixed value for r_e in ice clouds. According to (12), r_e increases from about 5×10^{-6} m when $W_i = 10^{-6}$ kg m^{-3} to about 110×10^{-6} m when $W_i = 10^{-4}$ kg m^{-3}. W_i is calculated from the in-cloud ice mixing ratio, i.e. $W_i = \rho q_i / C_i$, where C_i is the stratiform ice-cloud fraction. For ice clouds, the asymmetry parameter $\mathcal{G}_i$, which affects the ratio of forward-scattered to back-scattered short-wave radiation, is set to 0.8 in the control version of the scheme. This is the value suggested by Francis *et al.* (1994), although, as pointed out by these authors (and others), there is considerable uncertainty regarding the specification of $\mathcal{G}_i$. Stephens *et al.* (1990) used $\mathcal{G}_i = 0.7$ (a value which would result in increased backscatter and hence more reflective clouds), while the value for spheres (about 0.85) serves as an upper limit on the reasonable range of values for $\mathcal{G}_i$.

It is now well known that the treatment of clouds as plane-parallel by the radiation schemes used in GCMs results in an overestimate of cloud albedo (e.g. Harshvardhan and Randall 1985), so that GCMs have to predict artificially low cloud-water paths to achieve realistic albedos. Cahalan *et al.* (1994), in a study of marine stratocumulus during the First ISCCP (International Satellite Cloud Climatology Project) Regional Experiment (FIRE), found a 15% reduction in cloud albedo (compared to the plane-parallel values) because of horizontal liquid-water variability, and pointed out that the bias will be larger for other types of clouds which are less plane-parallel. They also suggested that reasonable estimates of the albedo could be achieved in models by multiplying cloud optical depths by a factor $\xi = 0.7$. Tiedtke (1996) included this modification in the model used by the European Centre for Medium-Range Weather Forecasts (ECMWF) and found improved agreement between the model's top-of-the-atmosphere short-wave fluxes and satellite observations. Kogan *et al.* (1995), based on three-dimensional large-eddy simulations of the evolution of a marine cloud-topped boundary-layer, found that $\xi \approx 0.5$ for cumulus and $\xi \approx 0.8$ for layer cloud. Guided by their results, the present scheme uses $\xi = 0.5$ for convective clouds, whereas for layer clouds ξ is increased linearly with stratiform-cloud fraction C, from a minimum value of 0.6 when $C = 0.2$ to a maximum value of 0.9 when $C = 0.8$.

The cloud emissivity is calculated as a function of infrared optical depth, and thus is a function of effective radius as well as liquid- (or ice-) water path (C. M. R. Platt, personal communication, 1994). Given the cloud visible optical depth $\delta_v = \beta_{ext}\Delta z$, with Δz the depth of the layer, the infrared optical depth is calculated as $\delta_a = 0.4\delta_v$ for water clouds or $\delta_a = 0.5\delta_v$ for ice clouds. The emissivity is then given by

$$\epsilon = 1 - \exp(-\mathcal{H}\delta_a) \tag{13}$$

with the optical depth diffusivity factor $\mathcal{H}$ approximated as 1.6 if $\delta_v > 0.4$ or 1.8 otherwise (derived from curves given by Platt and Stephens (1980)).

At temperatures between $-30\,^\circ$C and $0\,^\circ$C, cloud ice and cloud liquid water can coexist in the model, so it is necessary to specify the way in which ice and liquid water are mixed within a grid box. Sun and Shine (1994) showed that the radiative properties of mixed-phase clouds are sensitive to the method by which the phases are mixed, and pointed out that the choice of method could have a significant effect on the climate sensitivity of models that incorporate mixed-phase clouds. The three configurations they considered were 'uniform' (with ice and liquid water coexisting throughout the cloud), 'stratified' (with ice layers above the liquid-water layers) and 'adjacent' (with the cloud consisting of

two separate, vertically homogeneous clouds of single phase). They found that, for given amounts of cloud liquid water and cloud ice, the uniform method resulted in significantly higher cloud-albedos than the adjacent method. The adjacent method has been adopted in the scheme described here; this was also the method used by Mitchell *et al.* (1989). A number of other schemes have used the uniform method—there is currently no theoretical or observational basis for choosing between these two methods.

(*g*) *Fractional cloudiness and vertical overlap assumptions*

It is highly desirable that parametrizations for use in a GCM take into account fractional cloudiness, so that, for example, the 'in-cloud' values (rather than the grid-box-mean values) of the cloud-water mixing ratios are used in the calculation of precipitation. This avoids the problem encountered by Fowler *et al.* (1996), who had no treatment of fractional cloudiness and therefore had to use relatively low thresholds for the autoconversion of cloud water to precipitation. The parametrizations described here all use the cloud fraction calculated by the S90 condensation scheme to evaluate the mean in-cloud values of the required quantities. Clouds are assumed to be strictly randomly overlapped in the vertical, an assumption chosen for its simplicity and its consistency with the radiation scheme, although there is some observational evidence that maximum overlap is a better assumption for vertically adjacent cloud layers (Tian and Curry 1989). The parametrizations of precipitation and related processes are also developed on the assumption that all clouds completely fill their layers in the vertical, and that mixed-phase clouds are comprised of two horizontally adjacent clouds of single phase, again consistent with the methods used for calculation of the cloud radiative properties. (Thus, $C = C_i + C_l$, where C_i and C_l are the ice and liquid-water stratiform cloud fractions respectively.) It is also desirable that the parametrizations related to falling precipitation take into account the fraction of the grid box into which the precipitation falls, hereafter referred to as the *rainy* or *snowy* fraction. The calculation of this fraction is described in appendix C.

4. Parametrization of rain formation and related processes

In this section the modelled processes of rain formation (autoconversion, collection of cloud liquid water and evaporation of rain—see Fig. 1) are described and are compared with other schemes that have been used. The collection and evaporation parametrizations require assumptions about the fall speed and size distributions of raindrops—these are presented, together with observational evidence for the chosen formulations. The sensitivity of the rainfall processes to the time-step and numerics is also evaluated, by using a time-splitting approach in which the time-step used for the rainfall processes is varied independently of that used for other processes in the model in a series of 10-day experiments forced by climatological sea-surface temperatures (SSTs). The initial condition for each of these experiments was taken as 0000 UTC on July 1 in the second year of a model run performed using a version of the scheme very similar to the control version described here. The control experiment (hereafter referred to as 'CNTRL') used the version of the scheme described here, with no time-splitting, i.e. the usual model leapfrog time-step of 48 minutes was used for all the precipitation processes. Another experiment referred to is 'RAIN6', which was identical to CNTRL, except that the time-step used for the rainfall processes was reduced to six minutes. For experiments designed to evaluate the sensitivity of the rainfall processes to the time-step and numerics, differences from the RAIN6 run are shown, i.e. the RAIN6 run is used as the benchmark. For experiments designed to compare different parametrizations, differences from the CNTRL run are shown, since all of these experiments use the 48 minute time-step.

(*a*) *Autoconversion of cloud liquid water*

S90 parametrized the conversion of cloud liquid water to precipitation as the sum of an *autoconversion* term (Sundqvist 1978) and an *accretion* term which increases the conversion rate when precipitation (liquid or frozen) falls into the layer from above, viz.

$$(\dot{q}_l)_P = -C\left(c_T\left[1-\exp\left\{-\left(\frac{q_l/C}{c_W}\right)^2\right\}\right]+c_A P\right)\frac{q_l}{C}. \tag{14}$$

Here, using the notation of S90, c_T and c_A are rate constants for the autoconversion and accretion terms respectively, c_W is a critical mixing ratio at which the autoconversion process begins to be efficient and P is the rate at which precipitation falls into the layer from above. The parameters were given the values $c_T = 10^{-4}$ s^{-1}, $c_A = 1$ m^{2}kg^{-1} and $c_W = 8 \times 10^{-4}$ kg kg^{-1}, although more recent versions of the scheme have employed a reduced value of $c_W = 2 \times 10^{-4}$ kg kg^{-1} over the oceans, in order to improve the agreement between the liquid-water paths in the Meteorological Office model and satellite observations (Smith 1993). This parametrization has been widely used in large-scale models (Roeckner *et al.* 1992; Tiedtke 1993; Ricard and Royer 1993; Le Treut *et al.* 1994) although neither Sundqvist (1978) nor S90 gave any physical justification for its form.

An autoconversion parametrization with a stronger physical basis was derived by Manton and Cotton (1977), who used physical and dimensional arguments to improve upon the simple scheme of Kessler (1969), which has been used by Ose (1993) and Fowler *et al.* (1996). (See also Tripoli and Cotton (1980), hereafter TC80, in which the Manton and Cotton scheme was used in a cloud-resolving model in a study of cumulus clouds over Florida.) According to detailed calculations by J. B. Jensen (personal communication, 1995), the Manton and Cotton scheme gives more realistic rates of autoconversion than the Kessler scheme. In contrast to the Kessler scheme, which uses a simple formulation of the threshold, the Manton and Cotton scheme takes the cloud droplet concentration as an input parameter. The cloud droplet concentration can be parametrized as a function of the CCN concentration (e.g. Jones *et al.* 1994), which means that it can distinguish between the microphysics of maritime and continental clouds, and that it can be used to study the effects of anthropogenic production of aerosols on cloud microphysics. The parametrization, modified to allow for fractional cloudiness, takes the form

$$(\dot{q}_l)_{AU} = -C_l\frac{0.104 g E_{AU}\rho^{4/3}}{\mu(N_d\rho_w)^{1/3}}\left(\frac{q_l}{C_l}\right)^{7/3} H\left(\frac{q_l}{C_l}-q_{CR}\right) \tag{15}$$

where C_l is the liquid water cloud fraction, μ is the dynamic viscosity of air, ρ_w is the density of water, N_d is the droplet concentration, g is the acceleration under gravity, E_{AU} is the mean collection efficiency and ρ is the air density. H is the Heaviside unit step function which suppresses autoconversion until q_l/C_l reaches q_{CR}. The critical mixing ratio at which autoconversion begins is given by

$$q_{CR} = \frac{4}{3}\pi\rho_w r_{CR}^3 N_d/\rho \tag{16}$$

where r_{CR} is the critical mean droplet radius at which autoconversion begins. The present scheme uses $E_{AU} = 0.55$ (the same as the value used by TC80), $r_{CR} = 9 \times 10^{-6}$ m (slightly smaller than the value of 1×10^{-5} m used by TC80), $N_d = 5 \times 10^8$ m^{-3} for continental clouds and $N_d = 1 \times 10^8$ m^{-3} for maritime clouds (compared to $N_d = 3 \times 10^8$ m^{-3} as used by TC80). The slightly smaller value of r_{CR}, compared to that given by TC80, can be

TABLE 1. GLOBALLY AVERAGED, VERTICALLY INTEGRATED CONVERSION TERMS FOR RAINFALL PROCESSES (mm d^{-1}).

	RAIN6	CNTRL	implicit	explicit
autoconversion	0.068	0.079	—	0.083
collection	0.210	0.213	0.189	0.240
evaporation	0.209	0.214	0.203	0.225

The RAIN6 and CNTRL experiments are described in the text, while the columns labelled implicit and explicit refer to experiments identical to CNTRL, except that each individual term is treated implicitly or explicitly in turn.

justified by the much coarser spatial scales resolved by the GCM—autoconversion starts to become efficient when some droplets grow by diffusion to radii of around 20 μm (e.g. Mason 1975), and it seems reasonable to assume that this occurs at a smaller mean droplet-radius in a coarser resolution model such as a GCM. The use of different values of N_d for continental and maritime clouds is a simple way of allowing for the larger numbers of CCN in continental airmasses—a more sophisticated approach would involve parametrization of N_d as a function of the CCN concentration, the latter quantity probably being obtained from a chemical-transport model which provides the concentration of sulphate (and preferably other) aerosols as an output (e.g. Taylor and Penner 1994). A parametrization similar to (15) has been used recently by Boucher *et al.* (1995), who have described the sensitivity of their scheme to parameters such as N_d and r_{CR}. Note that the values of q_{CR} implied by (16) with r_{CR} and N_d as specified here are somewhat larger than the values used by Smith (1993) and many other existing schemes, especially over land.

Early experiments using a simple explicit evaluation of (15) showed a tendency for the scheme to overestimate the autoconversion rate, in the sense that negative liquid-water mixing ratios would be generated if not explicitly suppressed in the code. This was due to the large GCM time-step which is much greater than the time-steps for which the scheme was originally designed. A form more suitable for use with large time-steps is obtained by analytical integration of (15) with respect to time (see appendix B). This form of the parametrization prevents the generation of negative values and results in lower conversion rates than a simple explicit implementation of (15). A further modification is introduced to make the scheme more suitable for use with large time-steps: the autoconversion process is prevented from reducing the in-cloud liquid-water mixing ratio below q_{CR}. However, accretion of cloud liquid water by the raindrops generated by the autoconversion process is allowed to contribute to the conversion process (see appendix B), so that q_l/C can be reduced to less than q_{CR}. This approach is consistent with the finding of Berry and Reinhardt (1974a, b) that autoconversion initiates the process of conversion from small droplets to large drops, after which the conversion rate is dominated by accretion processes.

The zonal-mean autoconversion rates from the CNTRL run are shown in Fig. 6(a), with the differences of the CNTRL run from the RAIN6 run shown in Fig. 6(b). It can be seen that some increase in the autoconversion rates resulted from the increase of time-step from six minutes to 48 minutes. This was presumably because the autoconversion parametrization is invoked prior to the collection parametrization at each time-step. The globally averaged, vertically integrated values of the various conversion terms are shown in Table 1, which shows that the autoconversion term is, on average, roughly 16% larger in the CNTRL run compared to the RAIN6 run. As is shown below, the impact of this increase on the simulation is small, since the autoconversion term is quite small compared

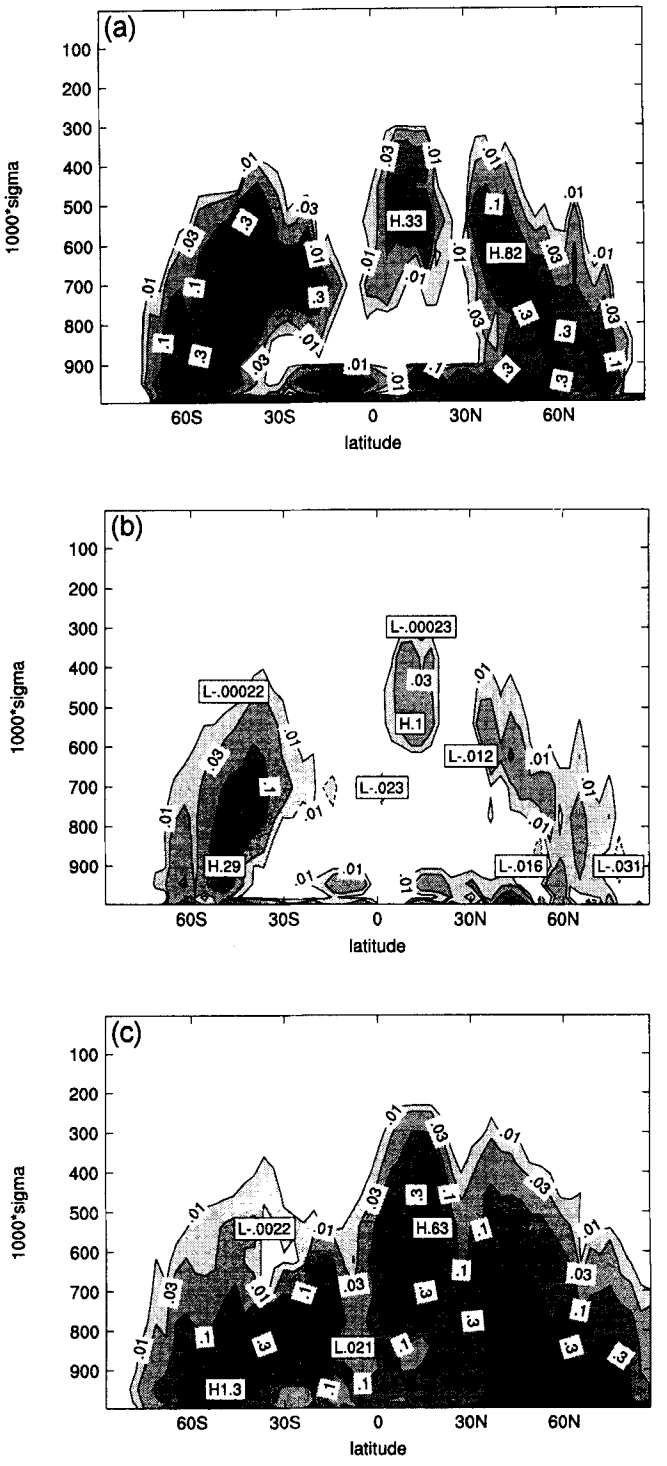

Figure 6. Time-averaged zonal-mean autoconversion rates (10^{-9} kg kg^{-1}s^{-1}) from various ten-day model experiments performed under July conditions. (a) CNTRL run; (b) differences of CNTRL run from RAIN6 run; (c) as (a), but autoconversion parametrized using (14) (differences from CNTRL run shown). Negative contours are dashed, and the depth of shading indicates the magnitude of the plotted values.

with those representing the other processes (collection, accretion) which deplete cloud liquid water. The globally averaged value for the explicit scheme given in Table 1 is just slightly larger than that from the CNTRL run. This experiment included the condition mentioned in the previous paragraph, preventing reduction of the in-cloud liquid-water mixing ratio below q_{CR}; without this condition, the explicit treatment gives much worse results.

Shown in Fig. 6(c) are the differences from the CNTRL run of the zonal-mean autoconversion rates from a run identical to CNTRL, except that autoconversion was parametrized using Sundqvist's (1978) scheme. In this run, the parameters were given the values used by S90, except that the critical mixing ratio q_{CR} at non-land grid-points was reduced to 2×10^{-4} kg kg^{-1}, as used by Smith (1993). Clearly, Sundqvist's scheme gave much larger autoconversion rates than the present scheme, with the parameters chosen as specified above. The globally averaged autoconversion-rate using Sundqvist's scheme was 0.182 mm d^{-1}, roughly 2.3 times larger than that in the CNTRL run. The mean autoconversion-rates are controlled both by the choice of q_{CR} and by the functional form of the parametrization—Sundqvist's scheme gave autoconversion rates somewhat more similar to the present scheme when used with values of q_{CR} based on (16) at each grid-point, with a globally averaged rate of autoconversion of 0.132 mm d^{-1}. These results are discussed in section 7.

(*b*) *Fall speed and size distribution of raindrops*

In this study, raindrops of diameter D_r are assumed to fall with terminal velocity

$$V_r(D_r) = k_r D_r^{1/2} \left(\frac{\rho_0}{\rho}\right)^{1/2} \tag{17}$$

where $k_r = 141.4$ m$^{1/2}$ s^{-1} and $\rho_0 = 1.2$ kg m^{-3} is a reference air density (RY88). This fall speed provides a good approximation to the observational data of Gunn and Kinzer (1949) in the range 1.2×10^{-3} m $< D_r < 4 \times 10^{-3}$ m.

There is a considerable body of observational evidence and some theoretical arguments (RY88) which suggest that the size distributions of raindrops (and ice particles) can be approximated by a negative exponential distribution, first suggested by Marshall and Palmer (1948). In this approximation, the number concentration of raindrops with diameters between D_r and $D_r + dD_r$ is $N_r(D_r)\, dD_r$, where

$$N_r(D_r) = N_{0r} \exp(-\lambda_r D_r). \tag{18}$$

The use of (18) is very convenient for the development of parametrizations, since it has the property that, for any non-negative real number x,

$$\int_0^\infty D_r^x N_r(D_r)\, dD_r = \frac{N_{0r}}{\lambda_r^{x+1}} \Gamma(x+1) \tag{19}$$

where $\Gamma(\,)$ denotes the gamma function. Marshall and Palmer found that the slope factor depends on the local rainfall rate R_r^l (kg m^{-2}s^{-1}) according to

$$\lambda_r(R_r^l) = 734(R_r^l)^{-0.21} \tag{20}$$

and that the intercept parameter is a constant, given by $N_{0r} = 8 \times 10^6$ m^{-4}. The present scheme uses this constant value for N_{0r}, in common with many other schemes (e.g. RH83; Lin *et al.* 1983; Fowler *et al.* 1996; Gregory 1995). The assumptions made here regarding

the fall speed and drop-size distribution imply a relation between the slope factor and the rainfall intensity, similar to (20). As shown in appendix B, this relation is

$$\lambda_r = 714 \left(\frac{\rho_0}{\rho}\right)^{1/9} (R_r^l)^{-0.22}, \tag{21}$$

which is similar to (20), deduced observationally by Marshall and Palmer (1948). This provides a useful check of the consistency of the parametrizations described in this subsection. Note that the alternative assumption of a constant slope-factor and variable intercept-parameter adopted by Tripoli and Cotton (1980) and Boucher *et al.* (1995) is more justifiable when very heavy rainfall rates, more typical of convective storms than large-scale precipitation, are being considered (e.g. Sauvageot and Lacaux 1995).

(c) *Collection of cloud liquid water by rain*

The rate of collection of cloud liquid water by falling rain is obtained by integration of the continuous-collection equation (which gives the rate of collection by a single raindrop) over the Marshall–Palmer distribution (18), together with the use of (17) for the fall speed of raindrops (see appendix B). After some minor simplifications (to save computer time) and evaluation of parameters, the parametrization takes the form

$$(\dot{q}_l)_{CO} = -0.24 f_r E_{CO} (R_r^l)^{3/4} q_l \tag{22}$$

where f_r is the rainy fraction of the grid box, E_{CO} is the mean collection efficiency and $R_r^l = R_r/f_r$ is the local rainfall rate. Measured collection-efficiencies are less than unity, and are generally an increasing function of both cloud-droplet and raindrop sizes (RY88). TC80 parametrized E_{CO} as a function of the Stokes number, based on an assumption of potential flow around the falling raindrop. A trial of their scheme in the CSIRO GCM yielded collection efficiencies that were generally in excess of 0.9, i.e. considerably larger than the measured values given by RY88. The present scheme uses the simpler approach of prescribing $E_{CO} = 0.7$, a value which is close to the measured data for 8 μm radius cloud droplets and essentially all raindrop sizes.

The control version of the scheme uses a centred-in-time method to evaluate q_l on the right-hand side (RHS) of (22) (see appendix B). With the centred-in-time approach, the modelled collection rates were quite insensitive to the time-step over the range tested, as shown in Fig. 7(a) (CNTRL run) and (b) (difference of CNTRL run from RAIN6 run). The differences shown in Fig. 7(b) can be partly attributed to the effect of the increased rates of autoconversion found in the CNTRL run compared to the RAIN6 run—in mid-latitudes, regions of decreased collection exist aloft (where collection and autoconversion compete for the available liquid water), with regions of increased collection below, where the rainfall released by autoconversion at higher levels collects liquid water. The globally averaged rates of collection, given in Table 1, are almost identical in the two runs. The effect of the choice of numerical scheme on the time truncation errors was also evaluated, via two other experiments. These were identical to the CNTRL run, except that q_l on the RHS of (22) was evaluated implicitly in one run and explicitly in the other. As is shown in Table 1, implicit evaluation of q_l resulted in collection rates which were, on average, 10% lower than those in the RAIN6 run. Conversely, explicit evaluation of q_l resulted in collection rates which were roughly 14% larger than those in the RAIN6 run. Analytical integration of (22), treating R_r^l as a constant, gave results similar to the centred-in-time approach, but the latter was preferred in order to save computer time.

Shown in Fig. 7(c) are the differences from the CNTRL run of the collection rates from another run identical to CNTRL, except that collection was parametrized according

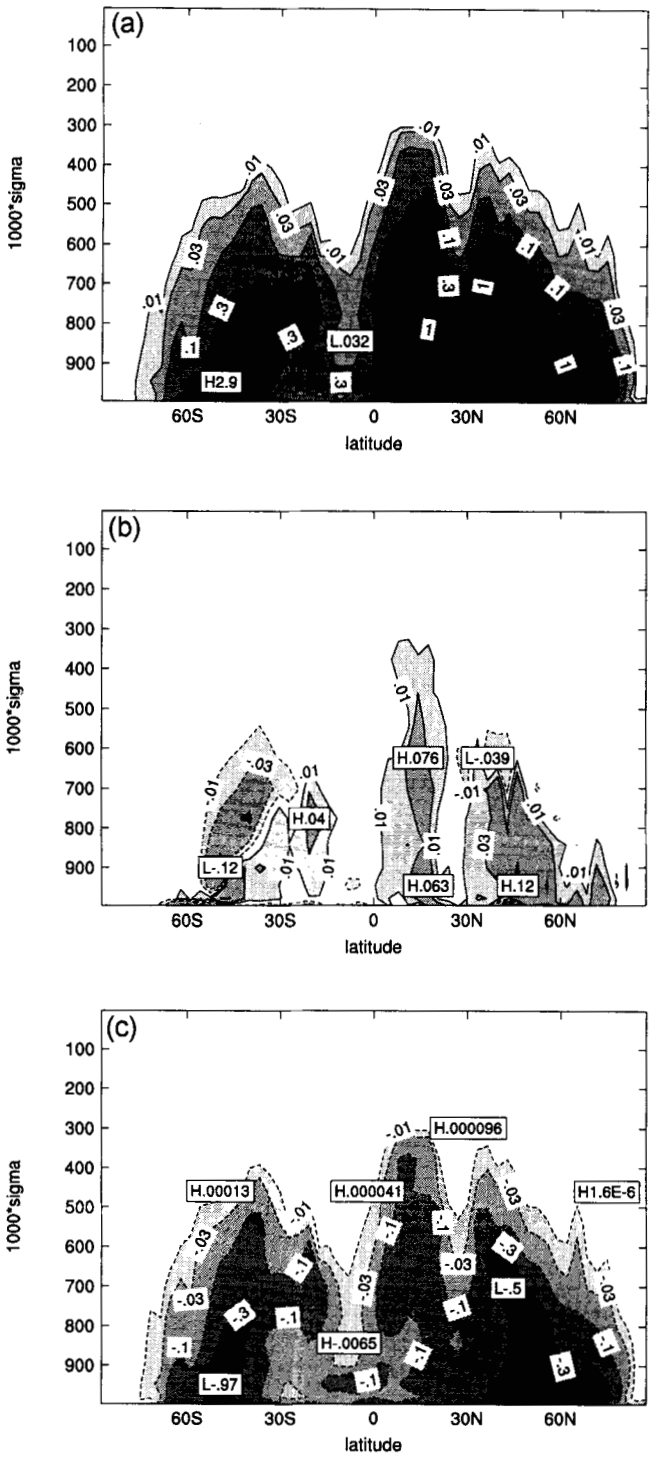

Figure 7. Time-averaged zonal-mean rates of collection of cloud liquid water by rain (10^{-9} kg kg^{-1}s^{-1}) from various ten-day model experiments performed under July conditions. (a) CNTRL run; (b) differences of CNTRL run from RAIN6 run; (c) as (a), but with collection parametrized using (14) (differences from CNTRL run shown). Negative contours are dashed, and the depth of shading indicates the magnitude of the plotted values.

to the scheme used by S90 (i.e. using the collection term in (14)). This parametrization resulted in somewhat lower collection rates than those generated by the present scheme, with a globally averaged value of 0.152 mm d^{-1}, roughly 29% lower than in the CNTRL run. (See discussion in section 7.)

(*d*) *Evaporation of rain*

The rate of change of water-vapour mixing ratio due to evaporation of rain is obtained by integration of the equation for the evaporation of a single raindrop of diameter D_r over the Marshall–Palmer distribution (18), together with the use of (17) for the fall speed of raindrops (see appendix B). After some minor simplifications and evaluation of parameters, the parametrization takes the form

$$(\dot{q}_v)_{EV} = f_r \frac{8.7 \times 10^2 (q_{sl} - q_v)}{\rho^{1/2}(A' + B')q_{sl}} (R_r^l)^{0.61} \tag{23}$$

where q_v is the water-vapour mixing ratio, A' and B' are temperature-dependent terms representing heat conduction and vapour diffusion respectively and other symbols are as defined previously. The experiments described in this paper use a computationally cheaper form of (23), in which $8.7 \times 10^2 (R_r^l)^{0.61}$ is approximated as $3.8 \times 10^2 (R_r^l)^{1/2}$.

A centred-in-time method is used to evaluate $(q_{sl} - q_v)$ on the RHS of (23) (see appendix B). With the centred-in-time approach, the modelled rates of evaporation were very insensitive to the time-step over the range tested, as shown in Fig. 8(a) (CNTRL run) and (b) (difference of the CNTRL run from the RAIN6 run). The globally averaged value, given in Table 1, is just slightly (2.4%) larger in the CNTRL run. This increase can probably be attributed to the increase in the amount of rain available for evaporation with the larger time-step (see Table 1). Two other runs, identical to the CNTRL run, except that $(q_{sl} - q_v)$ was evaluated implicitly in the first and explicitly in the second, were also performed. Compared to the RAIN6 run, the implicit scheme gave slightly (2.9%) reduced evaporation-rates, whereas the explicit scheme gave somewhat (8%) larger evaporation-rates (see Table 1). Although the magnitude of the average time-truncation errors obtained with the implicit scheme is not much different from that obtained with the time-centred scheme, the latter appears to be the better choice, as the errors obtained are in the direction expected from the slight increase in the amount of rainfall available for evaporation with the larger time-step. Further, theory suggests that the time-centred scheme will have smaller time-truncation errors. However, the differences are quite small compared to those resulting from the use of different parametrizations.

Shown in Fig. 8(c) are the differences from the CNTRL run of a run identical to the CNTRL run, except that evaporation of rain was parametrized using the scheme proposed by Gregory (1995). Gregory's scheme aimed to improve upon the simple formulation of Kessler (1969), and has been adopted in various forms in more recent versions (Smith *et al.* 1995) of the S90 scheme, which originally treated the evaporation of rain in a very simple manner. Gregory's scheme gives somewhat larger evaporation rates than the present scheme, with a globally averaged value of 0.252 mm d^{-1}, roughly 18% larger than that obtained in the CNTRL run. The evaporation rates obtained with Kessler's scheme (which has been used in large-scale models by Roeckner *et al.* (1992), Ose (1993) and Tiedtke (1993)) were larger again, with a globally averaged value of 0.260 mm d^{-1}. The version of Gregory's scheme mentioned above assumed a Marshall–Palmer drop-size distribution, as in the present scheme. Shown in Fig. 8(d) are the evaporation rates obtained using a modified version of Gregory's scheme, based on a gamma distribution of order 1. This version gave lower evaporation rates, which were quite similar to those produced by the

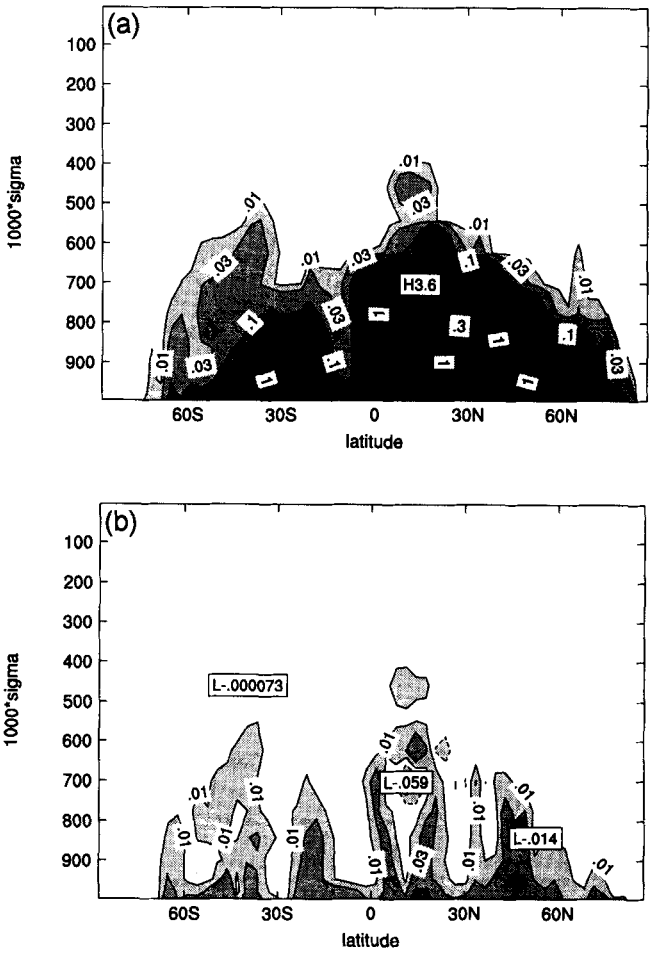

Figure 8. Time-averaged zonal-mean rates of evaporation of rain (10^{-9} kg kg^{-1}s^{-1}) from various ten-day model experiments performed under July conditions. (a) CNTRL run; (b) differences of CNTRL run from RAIN6 run; (c) as (a) but using Gregory's (1995) evaporation scheme with a Marshall–Palmer drop-size distribution (differences from CNTRL run shown); (d) as (c), but using a gamma drop-size distribution (differences from CNTRL run shown). Negative contours are dashed, and the depth of shading indicates the magnitude of the plotted values.

present scheme. The globally averaged evaporation rate for this run was 0.220 mm d^{-1}, just slightly larger than that obtained in the CNTRL run. (See discussion in section 7.)

(*e*) *Sensitivity of the modelled cloud-water and rainfall amounts to the time-step*

As shown above, the various terms related to large-scale rainfall (autoconversion, collection and evaporation) are quite insensitive to the time-step, provided that the numerical schemes used to calculate these terms are chosen carefully. This suggests that the modelled cloud-liquid-water contents and amounts of rainfall will also be insensitive to the time-step, justifying the decision to avoid using a time-splitting approach with a smaller time-step for the rain processes. Shown in Fig. 9(a) are the zonal-mean stratiform cloud-liquid-water mixing ratios from the CNTRL run, with the differences of the CNTRL run from the RAIN6 run in Fig. 9(b). The differences shown in Fig. 9(b) are small, especially in view of the uncertainties in the various parametrizations. The globally averaged,

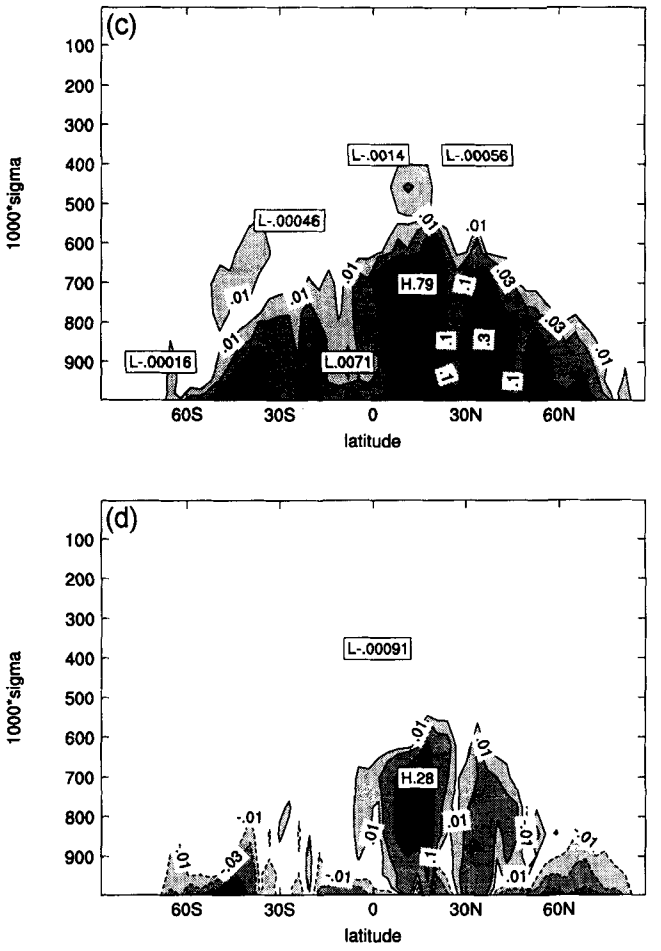

Figure 8. Continued.

vertically integrated cloud-liquid-water path is just slightly reduced due to the increase in time-step, from 0.0668 to 0.0665 kg m^{-2}. Also, the globally averaged large-scale rainfall differed by only 0.01 mm d^{-1} between these runs—the increase from 0.70 to 0.71 mm d^{-1} resulting from the increase in time-step can be attributed to the slightly increased auto-conversion rates obtained with the larger time-step. (Note that the figure of 0.71 mm d^{-1} for the CNTRL run can be recovered from Tables 1 and 2 as the sum of autoconversion plus collection plus flux divergence minus evaporation minus sublimation.) There was also a small corresponding decrease in the global-mean forcing of clouds by short-wave radiation, or short-wave cloud forcing (SWCF) of 0.1 W m^{-2}—these differences are small compared to the effects of replacing one parametrization by another.

There appears to be excessive cloud at very low levels in the model—a possible reason is that the model may be too moist at these levels. Although the modified Richardson number introduced with this cloud scheme has resulted in somewhat more vigorous vertical turbulent mixing of moisture, it may still be insufficient, since the model's turbulent-mixing-scheme is similar to a scheme which has been shown to lead to an excessively moist lowest level in the United States' National Center for Atmospheric Research (NCAR)

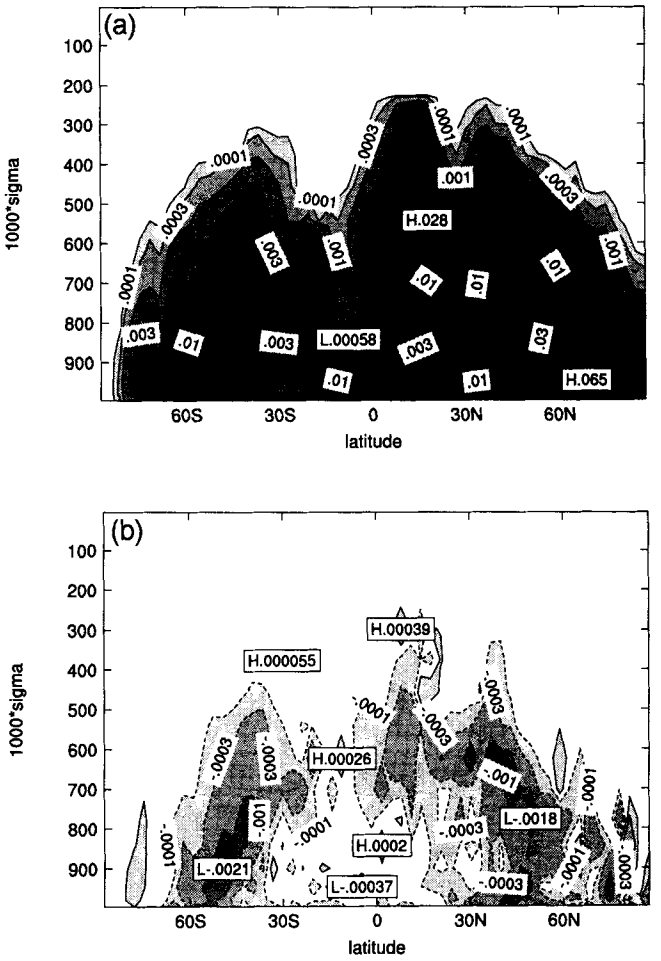

Figure 9. Time-averaged zonal-mean cloud-liquid-water mixing ratios (g kg^{-1}) from two ten-day model experiments performed under July conditions. (a) CNTRL run; (b) differences of CNTRL run from RAIN6 run. Negative contours are dashed, and the depth of shading indicates the magnitude of the plotted values.

TABLE 2. GLOBALLY AVERAGED, VERTICALLY INTEGRATED CONVERSION TERMS FOR FROZEN-PRECIPITATION PROCESSES (mm d^{-1}).

	SNOW6	CNTRL	implicit	explicit
flux divergence	0.911	0.848	0.824	0.100
accretion	0.514	0.482	0.458	0.490
sublimation	0.226	0.219	0.203	0.230

The SNOW6 and CNTRL experiments are described in the text, while the columns labelled implicit and explicit refer to experiments identical to CNTRL, except that each individual term is treated implicitly or explicitly in turn.

Community Climate Model (Holtslag and Boville 1993). Another possible reason is the use in the condensation scheme of a critical relative humidity RH_{CR} which does not vary with height—see the discussion in section 7.

5. Parametrization of frozen precipitation and related processes

In this section, the modelled frozen-precipitation processes (flux divergence of falling ice, accretion of cloud liquid water and sublimation of falling ice—see Fig. 1) are described and are compared with other schemes that have been used in GCMs. The assumptions regarding fall speeds and size distributions of ice particles are presented and evaluated against observations. The sensitivity of the ice processes to the choice of time-step and numerics is also evaluated, by comparison of the results from the ten-day CNTRL experiment described above with those from an otherwise identical run in which the time-step used for the ice processes was reduced to six minutes. This experiment is referred to as the 'SNOW6' run. For experiments designed to evaluate the sensitivity of the ice processes to the time-step and numerics, differences from the SNOW6 run are shown, i.e. the SNOW6 run is used as the benchmark. For experiments designed to compare different parametrizations, differences from the CNTRL run are shown, since all these experiments use a 48-minute timestep.

(*a*) *Precipitation of cloud ice*

A detailed treatment of precipitating ice (e.g. Lin *et al.* 1983) would include separate variables for pure ice crystals, snowflakes (aggregates of ice crystals) and graupel (heavily rimed ice particles). Hail can occur as an extremely dense form of graupel when the freezing of the accreted cloud-droplets is not immediate, and is generally produced only in the strong updraughts found in convective clouds. According to data shown by RY88, ice crystals typically fall at about 0.4–0.5 m s^{-1}, dry snowflakes at about 1 m s^{-1} and graupel particles at speeds greater than 1 m s^{-1}. In view of the computational demands of more sophisticated treatments, as well as the uncertainties associated with some of the terms in these schemes (especially the conversion of cloud ice to snow), a simpler approach is adopted in this study, in common with several other schemes (S90; Roeckner *et al.* 1992; Le Treut *et al.* 1994; Jakob and Morcrette 1995) that have been used in large-scale models. A single variable is used to represent all forms of atmospheric ice so that no real distinction is made between falling ice-crystals, snowflakes and graupel. Instead, the rate of precipitation of ice is parametrized using an empirical relation between the fall speed of ice and cloud ice content, derived from measurements made by Heymsfield (1977). Allowing for fractional cloudiness, this fall speed can be written as

$$\overline{V_f} = 3.23 \left(\frac{\rho q_i}{C_i} \right)^{0.17} . \tag{24}$$

The rate of change of cloud ice as a result of the flux divergence of falling ice is given by

$$(\dot{q}_i)_P = \frac{R_f}{\rho \Delta z} - q_i \frac{\overline{V_f}}{\Delta z} \tag{25}$$

where R_f is the rate at which ice falls into the layer from above (see appendix B) and Δz is the layer thickness. Explicit evaluation of (25) with the time-steps and vertical resolutions typical of current global models is liable to violate the Courant–Friedrichs–Levy criterion. Although an artificial limit to the flux leaving a layer can prevent values

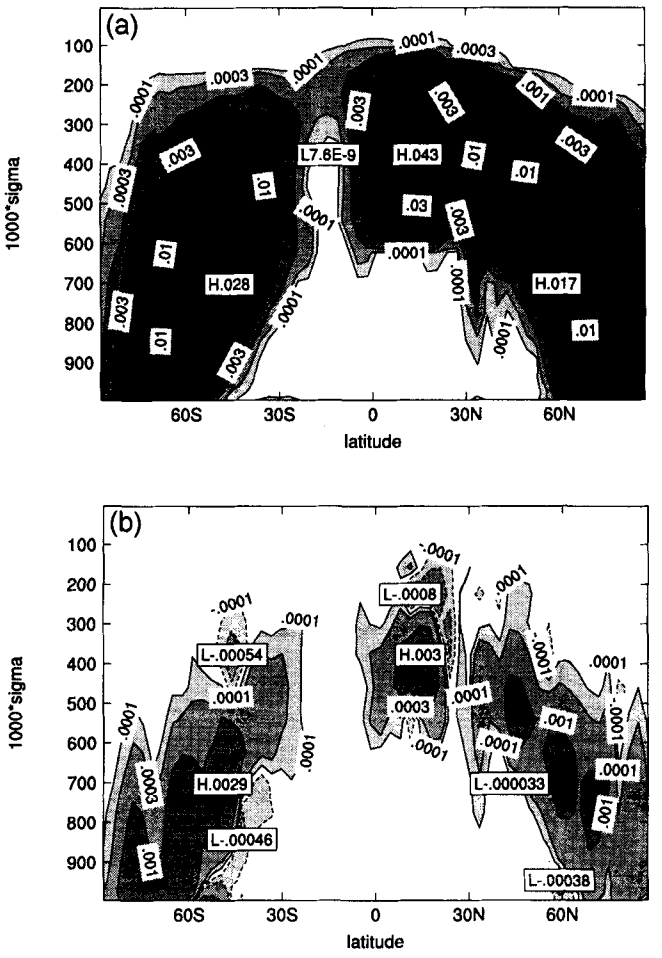

Figure 10. Time-averaged zonal-mean cloud-ice mixing ratios (g kg^{-1}) from various ten-day model experiments performed under July conditions. (a) CNTRL run; (b) differences of CNTRL run from SNOW6 run; (c) as (a), but using the 'fall-through' approximation (differences from SNOW6 run shown); (d) as (a), but using an implicit numerical scheme (differences from SNOW6 run shown). Negative contours are dashed, and the depth of shading indicates the magnitude of the plotted values.

of q_i becoming negative, to use one results in an underestimate of the precipitation rate (whenever $\overline{V_f}\Delta t > \Delta z$) and a consequent build-up of ice. In some recent studies, the problem has been addressed by adoption of a 'fall-through' assumption, (by ignoring the first term on the RHS of (25) (Senior and Mitchell 1993; Le Treut *et al.* 1994), or by making some other *ad hoc* assumptions (e.g. Jakob and Morcrette 1995). As is shown below, the 'fall-through' assumption leads to an overestimate of the precipitation rate and a corresponding underestimate of the cloud ice content, relative to that predicted by a more accurate evaluation of (25). Smith *et al.* (1995) used an implicit scheme for the evaluation of (25). This has the virtue of preventing the generation of negative values, and also allows the ice to fall through more than one model layer in a time-step, in contrast to explicit treatments. However, it is shown below that the implicit scheme results in an underestimate of the precipitation rate and a corresponding upward shift of the modelled cloud ice, compared to a more accurate analytical treatment.

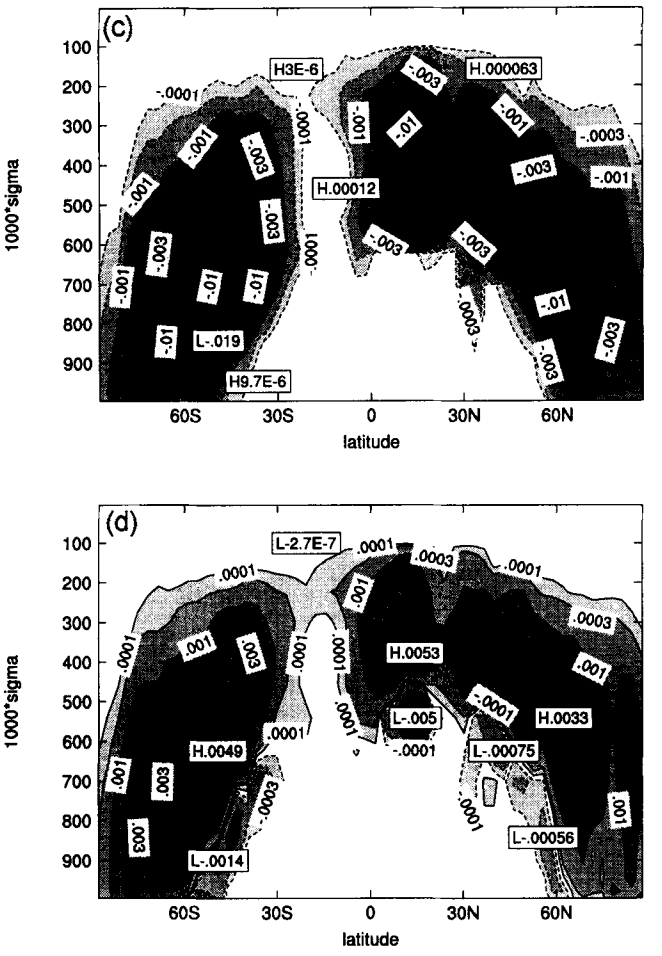

Figure 10. Continued.

The modelled cloud-ice mixing ratios are effectively controlled by the treatment of (25), rather than by the treatment of the accretion or sublimation terms described below, so cloud-ice amounts are shown as here as a proxy for $(\dot{q}_i)_P$. (The globally averaged values of the flux divergence $-(\dot{q}_i)_P$ are given in Table 2.) Figure 10(a) shows the zonal-mean cloud ice mixing ratios from the CNTRL run, with the differences of the CNTRL run from the SNOW6 run shown in Fig. 10(b). The use of the larger time-step resulted generally in a slight increase in the mean cloud-ice mixing ratios, although there are smaller regions of reduced cloud ice aloft and at low levels in mid-latitudes. The global-mean long-wave cloud radiative forcing (LWCF) for the CNTRL run was 29.8 W m^{-2}, in close agreement with the 29.7 W m^{-2} obtained in the SNOW6 run. Figure 10(c) shows the differences from the SNOW6 run of a run identical to the CNTRL run, except that the 'fall-through' approximation was made. The average cloud-ice mixing ratios obtained in this run were substantially lower than those in the SNOW6 and CNTRL runs and the global-mean LWCF was reduced to 27.6 W m^{-2}. Figure 10(d) shows the differences from the SNOW6 run of a run identical to the CNTRL run, except that (25) was evaluated implicitly. This run gave increased cloud ice aloft, with reduced cloud ice below, i.e. there was a systematic upward

shift of cloud ice associated with the implicit scheme, although the globally averaged value of the flux-divergence term is only slightly less than in the CNTRL run (see Table 2). A useful diagnostic of this shift is the global-mean LWCF, which increased to 32.0 W m^{-2} in the implicit run. Explicit evaluation of (25) was also found to be unsatisfactory at large time-steps (Table 2). Some improvement was obtained using a time-centred treatment, but the results (not shown) were still less satisfactory than those obtained with the analytically integrated scheme, which is also the best theoretically. Note that each of the numerical treatments of (25) implies that a certain fraction of the ice falling into a grid box during a time-step is allowed to fall through (see appendix B). So the use of this form is a natural way to determine the fraction of ice that falls through, rather than attempting to prescribe this fraction in some way.

(*b*) *Fall-speed and size distribution of falling ice particles*

The simplifying assumption that all ice particles fall with the mass-weighted mean velocity (24) is made in this study. Fall velocities of ice particles are a strong function of particle morphology as well as diameter (Locatelli and Hobbs 1974), but in general the exponent in a fall-speed relation analogous to (17) would be expected to be less than the value of 0.5 used for raindrops, because the density of ice particles tends to decrease with size. For example, RH83 used an exponent of 0.11 in their assumed relation between fall speed and particle diameter, while Lin *et al.* (1983) used an exponent of 0.25.

As with raindrops, the distribution of falling ice particles with size is assumed to follow a Marshall–Palmer distribution, so that the number concentration of falling ice particles with diameters between D_f and $D_f + dD_f$ is

$$N_f(D_f) = N_{0f} \exp(-\lambda_f D_f). \tag{26}$$

The assumption of a constant value for the intercept parameter N_{0f} is more difficult to justify for ice than for rain. Ryan (1996) showed plots of intercept parameter and slope factor as a function of temperature based on observations from a number of sources. Although there is considerable scatter, the data suggest that both N_{0f} and λ_f tend to increase with decreasing temperature and that λ_f can be parametrized as a function of temperature by

$$\lambda_f = 1.6 \times 10^3 \cdot 10^{0.023(T_0 - T)}. \tag{27}$$

By analogy with the arguments given in appendix B for rain, (27) implies a relation for the intercept parameter N_{0f}, viz.

$$N_{0f} = \left(\frac{\rho q_f / f_f}{\pi \rho_f} \right) \lambda_f^4, \tag{28}$$

where q_f is the mixing ratio of falling ice, f_f is the snowy fraction of the grid box (see appendix C) and ρ_f is the bulk density of ice particles (discussed below). Use of (28) in the model to diagnose N_{0f} from λ_f, gives values which are plotted against temperature in Fig. 11 and are broadly consistent with the data shown by Ryan (1996). The form of (27) was chosen to give reasonable agreement with these data, as well as with the observed values of λ_f. In the absence of suitable data at temperatures less than about −30°C, (27) is used at these lower temperatures also.

The bulk density of falling ice particles ρ_f is very uncertain. Ryan *et al.* (1976) found ice-crystal densities in cloud to lie in the range 400 kg m^{-3} to 900 kg m^{-3}, while Locatelli and Hobbs (1974) found a wide range of mass–diameter relationships for different types of precipitating ice particles, with the bulk density tending to decrease with increasing

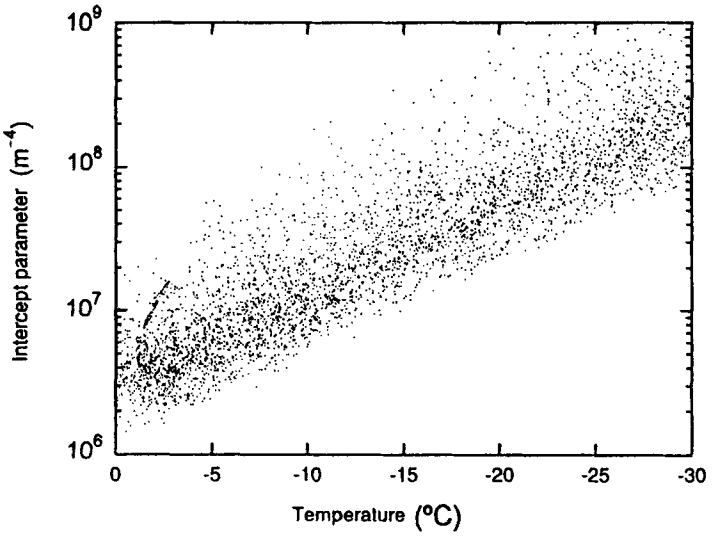

Figure 11. Scatter plot from a single model time-step showing the calculated intercept parameter N_{0f} for falling ice as a function of temperature.

size of particle, except for graupel, which had roughly constant density with size. Clough and Franks (1991) used several of these mass–diameter relationships in a one-dimensional model and found the corresponding mass-weighted mean particle densities to vary from around 20 kg m^{-3} to 400 kg m^{-3}. For parametrization purposes, ρ_f has typically been given a constant value of 100 kg m^{-3} (RH83; Lin *et al.* 1983; Gregory 1995), a value which is adopted for this study.

Falling ice is assumed to melt instantaneously to form rain when it enters a model layer which has a temperature of 2 °C or more, since observations show that snow usually melts in a layer of no more than a few hundred metres below the freezing level (Mason 1971). The assumption of instantaneous melting of snow has been made in most schemes used in large-scale models.

(c) *Accretion of cloud liquid water by falling ice*

The rate of accretion of cloud liquid water by falling ice is obtained by integration of the continuous-collection equation (which gives the rate of collection by a single ice particle) over the Marshall–Palmer distribution (26) (see appendix B). It has the conveniently simple form

$$(\dot{q}_l)_{AC} = -\frac{E_{AC}\lambda_f R_f q_l}{2\rho_f}, \tag{29}$$

where E_{AC} is the mean value of the collection efficiency and other symbols are as defined previously. The slope factor λ_f is parametrized as a function of temperature using (27). Real efficiencies for the accretion of cloud droplets by falling ice are again less than unity (Pitter and Pruppacher 1974), but are not well understood. Cotton *et al.* (1982) used an approach based on the Stokes number, similar to that used by TC80 for collection by raindrops. In the absence of a sufficiently simple and rigorous method for the parametrization of E_{AC}, the present scheme uses $E_{AC} = 0.7$. There is an additional source of uncertainty, because, as discussed above, the bulk density ρ_f of the ice particle is not as well defined as is the density of water ρ_w.

The control version of the scheme uses a centred-in-time method to evaluate q_l on the RHS of (29) (see appendix B). Shown in Fig. 12(a) are the zonal-mean rates of accretion from the CNTRL runs, with the differences of the CNTRL run from the SNOW6 run shown in Fig. 12(b). The differences resulting from the increase in time-step are quite strongly correlated with the differences in the downward flux of ice available for accretion of liquid water (not shown), with the choice of numerical scheme for the calculation of (29) having only a secondary effect. The globally averaged accretion rates are given in Table 2; the decrease of roughly 6% resulting from the increase of time-step from six minutes to 48 minutes is qualitatively consistent with the decrease in the flux-divergence term, which is the source of falling ice. Explicit evaluation of q_l on the RHS of (29), in conjunction with the 48-minute time-step, resulted in accretion rates that were slightly larger than those obtained in the CNTRL run, and in somewhat better agreement with the SNOW6 run. Conversely, an implicit scheme resulted in smaller accretion rates that were in worse agreement with the SNOW6 run. The variation with time-step of the downward flux of ice available to accrete liquid water makes it difficult to assess the relative merits of the schemes from these results, so the time-centred scheme has been chosen on theoretical grounds, and also because of the results obtained for the analogous collection term in section 4.

Shown in Fig. 12(c) are the differences from the CNTRL run of the accretion rates from a run identical to the CNTRL run, except that accretion of cloud liquid water by falling ice was parametrized using the S90 scheme (i.e. using the accretion term in (14)). This scheme resulted in much lower accretion rates than those obtained with the present scheme, with a globally averaged value of just 0.209 mm d^{-1}, i.e. 57% lower than in the CNTRL run. (See discussion in section 7.)

(*d*) *Sublimation of falling ice*

The rate of change of water-vapour mixing ratio due to sublimation of falling ice is obtained by integration of the equation for the sublimation of a falling ice particle of diameter D_f over the Marshall–Palmer distribution (26) (see appendix B). It has the form

$$(\dot{q}_v)_{SB} = \frac{4(q_{si} - q_v)}{\rho(A'' + B'')q_{si}} \left(\frac{R_f}{\pi\rho_f \overline{V_f}}\right) \left\{0.65\lambda_f^2 + 0.493\lambda_f^{3/2} \left(\frac{\overline{V_f}\rho}{\mu}\right)^{1/2}\right\}, \qquad (30)$$

where A'' and B'' are temperature-dependent terms representing heat conduction and vapour diffusion respectively, $\overline{V_f}$ is given by (24) and other symbols are as defined above. The slope factor λ_f is again parametrized as a function of temperature using (27).

As with the evaporation of rain, a time-centred scheme is used for the evaluation of $(q_{si} - q_v)$ on the RHS of (30). The zonal-mean rate of sublimation from the CNTRL run are shown in Fig. 13(a), with the differences of the CNTRL run from the SNOW6 run in Fig. 13(b). There was generally a slight decrease in the sublimation rates resulting from the increase in time-step, with the globally averaged value some 3% less in the CNTRL run (see Table 2). This is, again, qualitatively consistent with the reduction in the downward flux of ice resulting from the increase in time-step. The use of an explicit scheme gave sublimation rates which were in better agreement with the SNOW6 run at lower levels but which were too large in the tropical upper troposphere, whereas an implicit scheme gave sublimation rates which were lower than those from the SNOW6 run everywhere (not shown). Both theory and the globally averaged values given in Table 2 suggest that the time-centred scheme is again the best choice, bearing in mind the sign of the change expected because of the reduction in the available downward flux of ice.

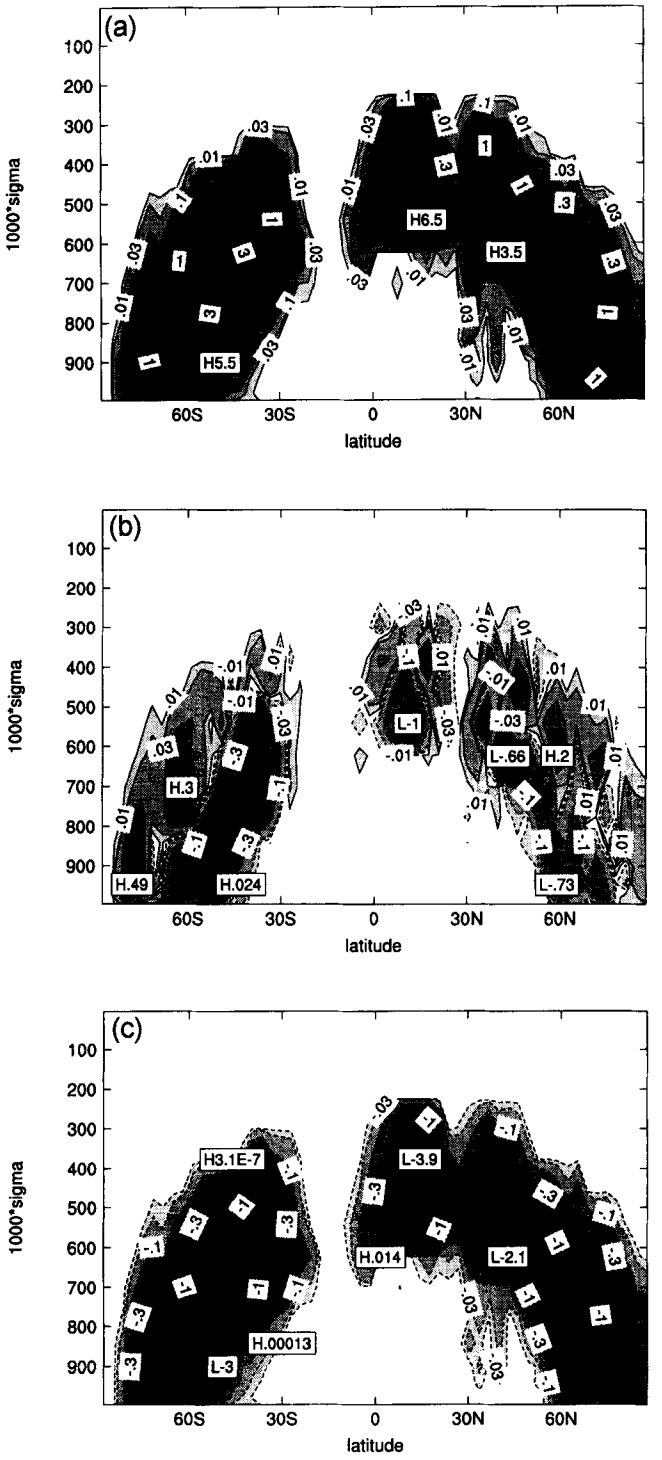

Figure 12. Time-averaged zonal-mean rates of accretion of cloud liquid water by falling ice (10^{-9} kg kg^{-1}s^{-1}) from various ten-day model experiments performed under July conditions. (a) CNTRL run; (b) differences of SNOW6 run from CNTRL run; (c) as (a), but with accretion parametrized using (14) (differences from CNTRL run shown). Negative contours are dashed, and the depth of shading indicates the magnitude of the plotted values.

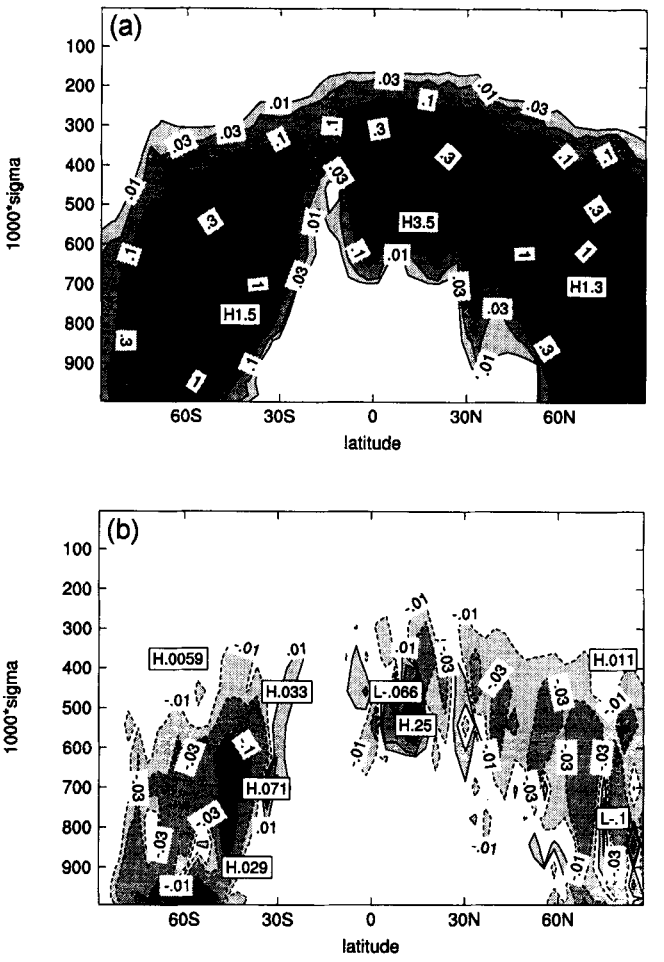

Figure 13. Time-averaged zonal-mean rates of sublimation of falling ice (10^{-9} kg kg^{-1}s^{-1}) from various ten-day model experiments performed under July conditions. (a) CNTRL run; (b) differences of CNTRL run from SNOW6 run; (c) as (a), but using Gregory's (1995) scheme (differences from CNTRL run shown); (d) as (a), but treating falling ice as rain (differences from CNTRL run shown). Negative contours are dashed, and the depth of shading indicates the magnitude of the plotted values.

Shown in Fig. 13(c) are the differences from the CNTRL run of the sublimation rates from a run identical to the CNTRL run, except that Gregory's (1995) scheme was used for the sublimation of falling ice. Compared to the present scheme, Gregory's scheme gave generally larger rates of sublimation (as much as 100% larger at low levels), in qualitative agreement with the earlier result regarding the evaporation of rain. However, at very low temperatures, Gregory's scheme gave lower sublimation rates than the present scheme. Figure 13(d) shows the differences from the CNTRL run of the sublimation rates obtained in a run identical to the CNTRL run, except that sublimation was calculated using (23), i.e. treating ice as rain. Much lower sublimation-rates were obtained in this run, with a globally averaged value of 0.132 mm d^{-1}, about 40% less than that from the CNTRL run. (See discussion in section 7.)

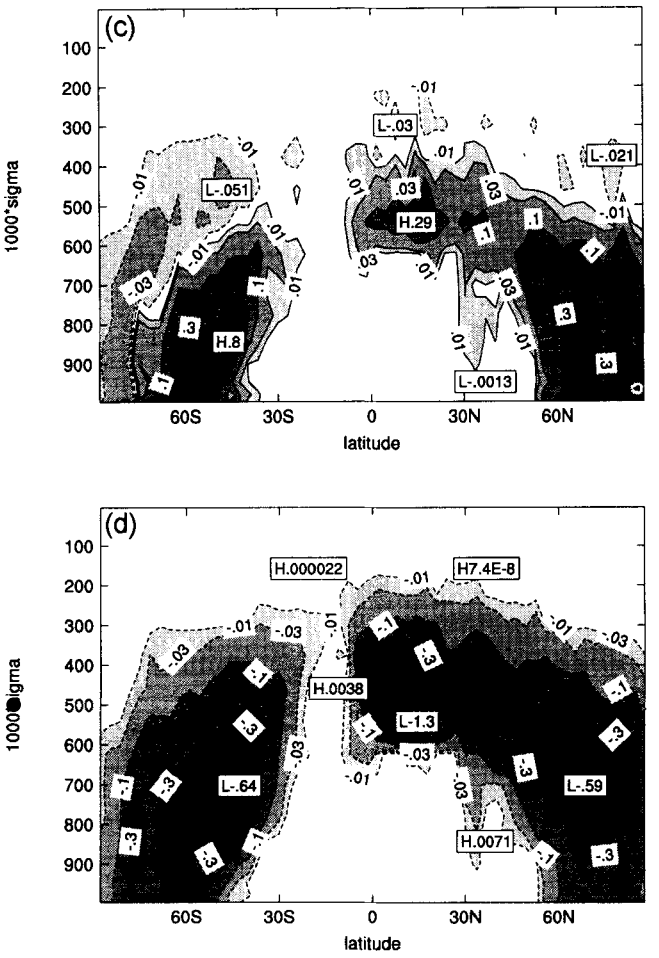

Figure 13. Continued.

6. Preliminary validation of large-scale cloud fields

In this section, a preliminary validation of a six-year run of the model, forced by climatological SSTs and using the control version of the scheme, is presented: zonal-mean fields averaged over July from the last five years of the run are shown and compared to appropriate observational data for July. This run will be analysed in more detail in Part II. Also shown, for comparison, are zonal-mean cloudiness and cloud radiative forcing from a 10 year run which used the standard Mark 2 version of the model (described in section 2). Other than inclusion of the prognostic cloud scheme and the increase of vertical resolution, the only significant difference between the two versions of the model is the treatment of shallow convection, which follows Geleyn (1987) in the standard model and Tiedtke (1988) in the version with the prognostic cloud scheme. The two model experiments are referred to as the 'PROG' and 'DIAG' runs respectively.

Figure 14 shows July zonal-mean total cloudiness from the two model runs, along with the D2 data from ISCCP (Rossow *et al.* 1996) averaged over the period 1990 to 1992 and surface observations (land and ocean combined) from Warren *et al.* (1986, 1988). The

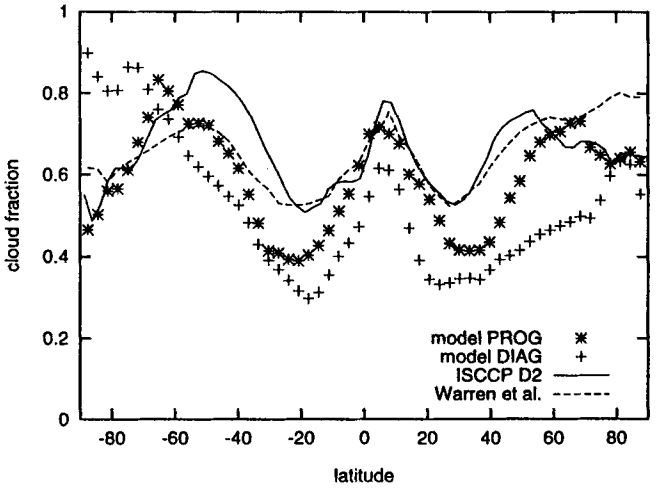

Figure 14. July zonal-mean cloudiness from the model, using the present scheme (PROG) and the diagnostic cloud scheme (DIAG), and from observations.

global-mean cloudiness from the DIAG run is 47%, less than the observed values of 66% from ISCCP and 63% from Warren *et al.*, whereas the PROG run has a more realistic value of 57%. The zonal-mean distribution of cloudiness from the PROG run also shows improved agreement with the observed data. The peaks in cloudiness associated with mid-latitude storm tracks are captured more realistically in the PROG run, and the cloudiness over Antarctica appears to be more realistic, even bearing in mind the uncertainty in the observations at high latitudes. However, cloud cover in the model is still too low in the subtropics and mid-latitudes (in common with many other models). Preliminary experiments (not shown) with a 24-level version of the model (including an additional 2 levels below $\sigma = 0.8$) have considerably more cloud cover in the subtropics, suggesting that a lack of vertical resolution at the boundary layer at least partly causes the deficiency of subtropical cloud in the 18-level version.

Figure 15 shows the zonal-mean variation of the liquid-water paths from the PROG run averaged over ocean points for July, together with Special Sensor Microwave/Imager (SSM/I) observations retrieved by the algorithms of Greenwald *et al.* (1993) and Weng and Grody (1994). The data of Greenwald *et al.* are averaged over the period 1987 to 1991, whereas those of Weng and Grody are averaged over the period 1987 to 1995. Unfortunately, the observed liquid-water paths are very uncertain at present—the liquid-water paths retrieved by Weng and Grody are substantially lower than those of Greenwald *et al.*, with a global-mean value over oceans of 0.062 kg m^{-2} compared to 0.084 kg m^{-2}, and much lower values in the subtropics. In the southern hemisphere, the modelled liquid-water paths agree quite well with the values of Weng and Grody, but are too low compared to those of Greenwald *et al.* In the northern hemisphere, the modelled values agree quite well with those of Greenwald *et al.*, but are too large compared to those of Weng and Grody. The modelled values are somewhat too large in mid-latitudes, compared to both sets of observations. In the tropics, the peak in the modelled values appears to be too broad. The global-mean liquid-water path over oceans in the model is 0.076 kg m^{-2}, in between the global-mean values from the two sets of observations.

The zonal-mean LWCF (calculated using method 2 of Cess *et al.* 1992) from both model runs is shown in Fig. 16, together with observed data from the Earth Radiation

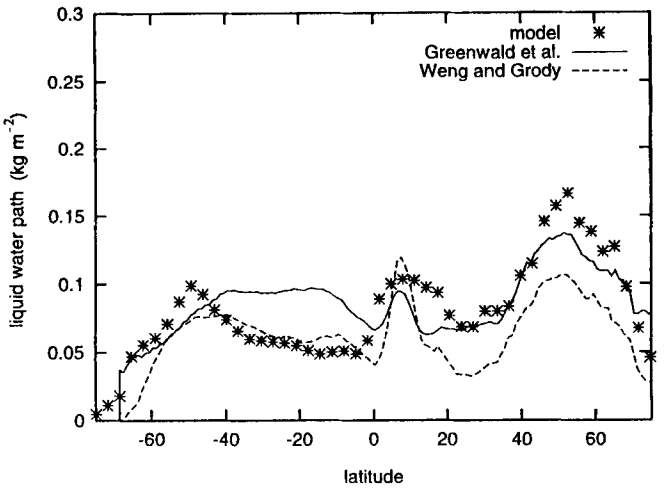

Figure 15. July zonal-mean liquid-water path over oceans from the model and from satellite observations.

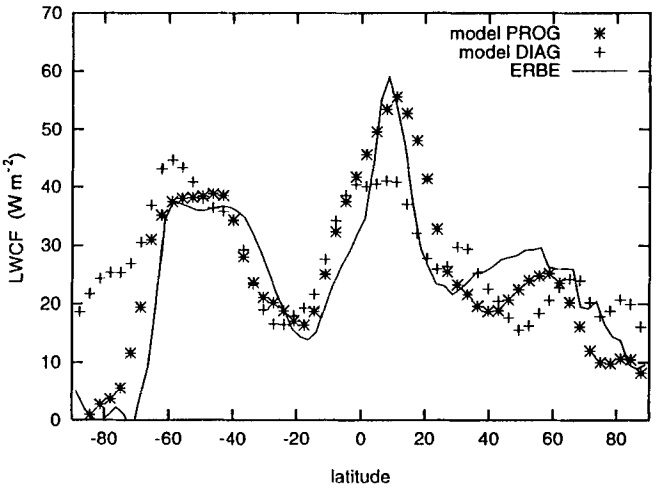

Figure 16. July zonal-mean LWCF from the model, using the present scheme (PROG) and the diagnostic cloud scheme (DIAG), and from ERBE.

Budget Experiment (ERBE) averaged over the period 1985 to 1989. The ERBE cloud-forcing fluxes are considered to be quite uncertain poleward of about 60° latitude, and should be regarded with caution there. The global-mean LWCF is 28.9 W m^{-2} in the DIAG run and 29.9 W m^{-2} in the PROG run, both in close agreement with the ERBE value of 28.4 W m^{-2}. However, the zonal-mean distribution in the PROG run is more realistic than in the DIAG run, particularly in the tropics and over Antarctica. Even in the PROG run, some deficiencies are evident: the modelled LWCF is somewhat weaker than the LWCF from ERBE in northern hemisphere mid-latitudes, and the peak in the tropics again appears to be too broad.

The zonal-mean (method 2) SWCF from both model runs is shown in Fig. 17, together with data from ERBE averaged over the period 1985 to 1989. The global-mean SWCF is

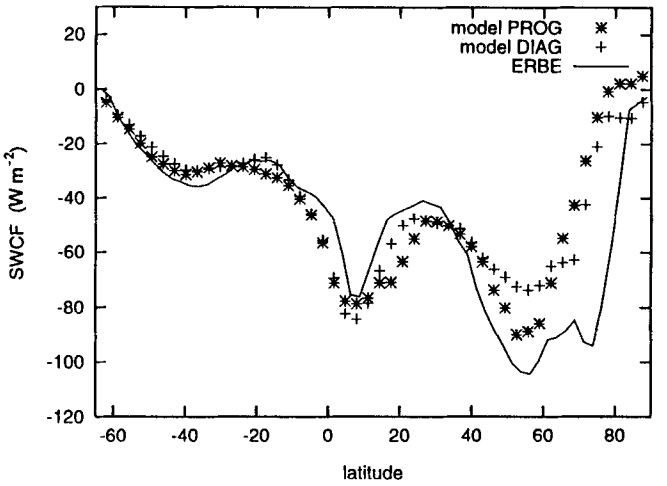

Figure 17. July zonal-mean SWCF from the model, using the present scheme (PROG) and the diagnostic cloud scheme (DIAG), and from ERBE.

-43.5 W m^{-2} in the DIAG run and -45.6 W m^{-2} in the PROG run, both in reasonable agreement with the ERBE value of -47.9 W m^{-2}. The zonal-mean distributions from the two runs do not differ greatly, and agree well with the observations, except in the northern hemisphere mid-latitudes, where the modelled SWCF is too weak in both runs (in common with most other models). In this region, the SWCF from the PROG run is noticeably more realistic than that from the DIAG run. Polewards of about 65°N, the SWCF from the PROG run appears to be slightly worse, but this turns out to be the result of excessive snow and sea-ice that is retained in July in the PROG run, and which reduces the modelled SWCF because it provides a highly reflective surface underneath the clouds. The SWCF from both runs is also somewhat too strong in the tropics, again in common with most other models. Some possible explanations for the deficiencies in the SWCF from the PROG run are suggested in the next section.

7. Summary and discussion

(*a*) *Summary of scheme*

The preceding sections have described a prognostic scheme for the treatment of stratiform clouds and precipitation, intended for use in GCMs and other large-scale models. The scheme incorporates prognostic variables for cloud liquid water and cloud ice, and includes the following components:

- a simple 'statistical' scheme for the formation and dissipation of cloud—the equations for calculation of the cloud fraction and the amount of condensed water are given by Smith (1990);
- a novel approach to the determination of the liquid-water fraction in mixed-phase clouds, driven primarily by the relative difference between the saturation mixing ratios with respect to ice and water (section 3(c));
- semi-Lagrangian advection and vertical turbulent mixing of cloud liquid water and cloud ice—these terms have a relatively minor effect on the simulation (section 3(d));
- initiation of rain by autoconversion, using a parametrization which can distinguish between the microphysics of maritime and continental clouds (Eq. (15));

- an observationally based fall-speed for ice particles (Eq. (24)), which is used to calculate the rate of precipitation of cloud ice as the flux divergence of falling ice (Eq. (25));
- accretion of cloud liquid water by falling rain and ice, derived from the continuous-collection equation using observationally based (Marshall–Palmer) size distribution for raindrops and ice particles (Eqs. (22) and (29));
- evaporation of rain and falling ice, parametrized by integration of the equation for evaporation of a single raindrop (or ice particle) over the appropriate Marshall–Palmer size-distribution (Eqs. (23) and (30));
- parametrization of cloud effective radius as a function of liquid water content and cloud droplet concentration for warm clouds (Martin *et al.* 1994) or as a function of ice water content for cold clouds (Eq. (12));
- calculation of cloud radiative properties from the liquid- (or ice-) water path and effective radius, following Slingo (1989) for the short-wave properties and using (Eq. (13)) for the emissivity.

The scheme has been implemented and tested in an R21, 18-level version of the CSIRO, combined with a simple diagnostic treatment of convective clouds. During the development of the scheme, considerable attention was paid to the physical principles underlying the various parametrizations, especially those related to precipitation, while simultaneously trying to provide a scheme with moderate computational overheads.

(*b*) *Choice of time-step and computational overheads*

The sensitivity of the precipitation processes to the time-step used for their calculation was evaluated in a series of short GCM experiments, to determine whether it is necessary to use a reduced (split) time-step of six minutes for the cloud microphysics, or whether the usual 48-minute leapfrog time-step is sufficiently small. (Note that the scheme which calculates the formation and dissipation of cloud does not use a time-step.) The experiments showed that the various terms are not very sensitive to the time-step, provided that some of the numerical schemes used for their evaluation are chosen with care. Theoretically, time-centred differencing was expected to give smaller time-truncation errors than implicit or explicit differencing in the evaluation of the collection, evaporation, accretion and sublimation terms. For the rainfall processes (i.e. collection and evaporation), these expectations were clearly borne out by the GCM experiments, whereas for the ice processes (i.e. accretion and sublimation) it was more difficult to assess the relative merits of the various schemes, because the available downward flux of ice varied with the change of time-step. For the calculation of autoconversion, an analytical treatment gave better results than a simple explicit treatment. The choice of numerical scheme was found to be important in the calculation of the flux divergence of falling ice, where the use of an implicit scheme for the calculation of the flux divergence resulted in an increase of more than 2 W m^{-2} in the global-mean LWCF, compared to a more accurate analytical scheme, which showed little variation (0.1 W m^{-2}) over a wide range of time-steps. Another scheme that has been used in global models (the 'fall-through' approximation) resulted in a decrease of more than 2 W m^{-2} in the global-mean LWCF. The excellent result obtained with the analytical scheme suggests that it is the natural way to handle the calculation of the flux-divergence of ice implied by (24), especially at large Courant numbers. Overall, the results support the conclusion that the cloud microphysics does not require the use of a split time-step, which would entail considerable computational overheads. Higher resolution (R42 or T63) versions of the GCM would use a time-step half that of the low-resolution version used here and would improve the results obtained for the frozen precipitation, which showed

some sensitivity to the time-step. One question this study has not addressed is whether the diagnostic treatment of rainfall is satisfactory, or whether the results would be substantially altered by treating rain as a prognostic variable, as is done in some other schemes. With this qualification, the present results suggest that it is not necessary to use a split time-step in the relatively simple microphysical schemes which are typically used in current GCMs. This conclusion may not hold for more complex schemes (Ghan and Easter 1992; Fowler *et al.* 1996).

Inclusion of the control version of the prognostic cloud-scheme in the R21, 18-level model increases the computer time needed from about 221 seconds to about 305 seconds per model day on a single processor of a Cray J916 mini-supercomputer. Of this increase of 38%, a little less than half (18%) is the result of the cloud microphysical processes shown in Fig. 1, with the bulk of the remainder resulting from increased overheads in the radiation scheme, including the increased number of cloud layers and interactive calculation of cloud radiative properties (10%) and the semi-Lagrangian advection of cloud water (5%). If a six-minute time-step is used for the precipitation processes, the overhead caused by microphysical processes increases from 18% to 65%. The overhead of 38% for the entire scheme is regarded as reasonable, especially in view of the modest computational demands of the standard version of the CSIRO GCM relative to some other GCMs. Also, with increased horizontal resolution, the cloud scheme is expected to account for a lower percentage of the model's total requirement than it does at R21, since the spectral transforms will become relatively more expensive, while the number of time-steps between calls to the radiation scheme will increase. The overhead of 38% also compares very favourably with the scheme of Fowler *et al.* (1996) which caused a doubling of the computer time required to run the CSU GCM, from 110.5 to 220.2 seconds per model day on a Cray C-90. The CSU GCM has 17 vertical levels and horizontal resolution of 4° by 5°, i.e. slightly lower resolution overall than the 18-level R21 model used in the present study. Based on tests performed with the CSIRO GCM, the processors on the C-90 are approximately four times faster than those on the J916, so the overhead for the present scheme of 84 seconds per model day on the J916 would translate to about 21 seconds per model day on the C-90, i.e. more than five times faster than the figure of 110 seconds given by Fowler *et al.* (1996). Alternatively, inclusion of the Fowler *et al.* scheme in the CSIRO GCM would roughly triple the computer time required to run a model day, relative to the version with the diagnostic cloud scheme.

(*c*) *Comparisons with other schemes*

In a further series of short GCM experiments, the parametrizations of the processes which remove cloud liquid water were compared with (14), which was used by Smith (1990) and subsequently in a number of other models. Compared to (14), the present scheme gave considerably lower rates of autoconversion, slightly higher rates of collection by falling rain, and considerably higher rates of accretion by falling ice. The lower autoconversion rates resulting from the present scheme arose from both the larger critical mixing ratios used and the differing functional form of the parametrization. The larger accretion rates can be explained by the lower density of falling ice particles compared to raindrops—this difference is not accounted for in the Smith scheme, which treats all falling precipitation identically. Putting the density of ice particles lower than that of raindrops in (29) results in larger accretion rates for a given downward flux of ice. The combination of a smaller autoconversion term and a larger accretion term, as used in the present scheme, is more consistent with the accepted view (e.g. Rutledge and Hobbs 1983) that ice processes are responsible for most of the precipitation produced in frontal clouds. The method used here to determine the relative amounts of liquid water and ice in mixed-phase clouds also

appears to be more realistic than the simple interpolation in temperature used in earlier schemes, since the present method does not allow ice to melt spuriously at sub-freezing temperatures, and generates liquid-water fractions that agree fairly well with observations. However, the treatment of mixed-phase clouds used here is still quite simple—some deficiencies are noted below.

The remaining experiments were designed to permit comparison of the rates of evaporation of precipitation produced by the present scheme with those produced by other schemes (Kessler 1969; Gregory 1995) that have been used in large-scale models. The present scheme gave lower rates of evaporation of rainfall than the other schemes, and lower rates of sublimation of falling ice than Gregory's scheme. (Kessler's scheme did not include ice processes.) According to Gregory (1995), his scheme gave rainfall evaporation rates which were too large when compared to the detailed microphysical calculations of Clough and Franks (1991) when a Marshall–Palmer drop-size distribution was used in the derivation of the scheme. An explanation proposed by Gregory involved the form of the drop-size distribution, since he obtained better agreement with the results of Clough and Franks when a gamma distribution of order 1 was used. When tested in the CSIRO GCM, this version of Gregory's scheme gave rates of evaporation similar to those obtained with the present scheme. Comparison of the physical basis of the present scheme with that of Gregory's scheme suggests a possible explanation for the lower evaporation rates produced by (23), despite the use of a Marshall–Palmer distribution. In the derivation of his scheme, the temperature at the surface of an evaporating drop is approximated by the wet-bulb temperature, whereas (23) is based on the (approximate) simultaneous solution of the equations for diffusion of vapour away from and heat towards the surface of an evaporating drop (Mason 1971). Use of the wet-bulb temperature is known to result in an overestimate of the evaporation rate (J. D. Kepert, personal communication, 1995), so this is another possible reason for the larger evaporation rates produced by Gregory's scheme. Kessler's (1969) scheme is based on an even simpler approach, in which the variations with temperature of the diffusivity and other quantities are ignored. The differences between the results obtained for the sublimation of falling ice using Gregory's scheme and the present scheme may possibly be explained similarly in terms of the use of the ice-bulb temperature in the development of his parametrization, although further investigation would be required to explain the interesting variation of the differences with temperature. A final experiment tested the effect of treating the sublimation of falling ice as evaporation of rain, which resulted in considerably reduced sublimation rates. This result is consistent with the finding of Clough and Franks (1991) that most forms of ice evaporate more efficiently than rain, primarily due to the lower density of ice particles. This is not accounted for in some schemes (e.g. Sundqvist *et al.* 1989; Ose 1993; Tiedtke 1993) which treat the evaporation of all precipitation identically.

(*d*) *Some uncertainties in the scheme*

The method used in the present scheme to determine the liquid-water fraction in mixed-phase clouds is driven primarily by $(q_{sl} - q_{si})/q_{si}$, i.e. by the relative difference between the saturation mixing ratios with respect to liquid water and ice, which increases with decreasing temperature. This quantity also appears as a key parameter in the physically based parametrization discussed in appendix A. The encouraging agreement between the modelled liquid-water fractions and observations shown in Fig. 5 suggests that, in the mean, this relative difference is the primary factor that controls the observed variation of liquid-water fraction with temperature, although in individual clouds other factors (such as IFN concentration and droplet-size distribution) will be important too. It was argued in section 3 that the present approach is more realistic than the interpolation in temperature

used in earlier schemes, but it still has some deficiencies. While it includes a physically based treatment of accretion of liquid water by falling ice particles, the other process by which falling ice-particles grow, namely by vapour deposition in regions of supercooled water, is not explicitly treated in the scheme, since an obvious method of parametrizing this process (appendix A) was found to be inconsistent with assumptions made in the cloud-formation scheme. The somewhat higher liquid-water fractions generated by the simple scheme used here (as compared with aircraft observations in stratiform cloud) suggest that inclusion of further processes that convert liquid water to ice would improve the results, particularly in deep frontal clouds, which are more likely to be glaciated (Bower *et al.* 1996). It may also be helpful to include some treatment of ice-multiplication processes, which can result in explosive growth of the number concentration of ice crystals, but are not fully understood (Rogers and Yau 1988). Another issue is the assumption that sufficient condensation occurs to remove any supersaturation with respect to ice; this assumption is made in the cloud formation scheme and carried through to the treatment of mixed-phase clouds. The assumption (which is made in many GCMs) is questionable, since the lack of IFN in the real atmosphere means that the air in ice clouds can be significantly supersaturated with respect to ice (Heymsfield and Miloshevich 1995). One effect of the assumption in the present scheme is that, at temperatures just below 0 °C, the model may produce pure ice clouds if the atmosphere is supersaturated with respect to ice but subsaturated with respect to water, whereas, in nature, ice production at these temperatures generally occurs via the freezing of water droplets. This is less of a problem in practice than in theory, because at these temperatures $(q_{sl} - q_{si})/q_{si}$ is small, and it is only in grid boxes with very small cloud fractions that this situation can occur (i.e. the cloud fraction would have to be smaller than the light grey area in Fig. 2). In practice, the modelled liquid-water fractions (see Fig. 5) are generally large at temperatures close to 0 °C, and, if anything, are larger than the observed values. The treatment of mixed-phase clouds in large-scale models remains very uncertain, and more work is needed to establish improved parametrizations of the key processes.

Another uncertainty in the present scheme is the formation and dissipation of cloud, treated using a simple statistical condensation scheme (Smith 1990). The scheme in its present form (using an arbitrary critical relative humidity to specify the sub-grid variability of the moisture distribution) is a rather simple approach to the problem, and lacks a clear physical basis for selection of the critical relative humidity. The use of a fixed RH_{CR} which does not vary with height was also identified as a possible cause of the excessive cloud generated by the scheme in the lowest one or two layers of the model. The use of larger values of RH_{CR} in the lowest one or two layers would ameliorate this problem, but this approach was avoided in view of the lack of a sound basis for the choice of RH_{CR} and the intention to implement a more sophisticated treatment in a future version of the scheme. More sophisticated versions of the condensation scheme have been tried, for example the scheme of Ricard and Royer (1993), in which the sub-grid variance of moisture is parametrized as a function of the Richardson number calculated by the model's turbulent-mixing scheme. Ideally, in a large-scale model, the sub-grid moisture variance should also depend on unresolved mesoscale motions, which could possibly be parametrized as a function of the model's grid spacing (Ek and Mahrt 1991). The possibility of upgrading the scheme as indicated remains an attractive possibility, as a more explicit treatment of condensation and evaporation of cloud water on the scale of a GCM grid-box is a difficult problem, because of uncertainties in how to calculate the cloud fraction and morphology, the amount of mixing between cloudy and environmental air and, at sub-freezing temperatures, the number concentration of ice crystals. Alternative condensation schemes which also allow fractional cloudiness have been presented by Sundqvist (1978)

and Tiedtke (1993), although neither of these schemes completely avoids the use of an arbitrary critical relative humidity. Another question regarding the condensation scheme is whether it is appropriate when coupled to a convection scheme that includes a more realistic treatment of anvil cirrus clouds—these clouds have long lifetimes and can be advected over long distances, yet the scheme assumes instantaneous evaporation of cloud when the relative humidity drops below the critical value.

The critical relative humidity RH_{CR} used by the condensation scheme is one of several parameters in the present scheme which are very uncertain; other such parameters are the critical droplet-radius r_{CR} used by the autoconversion parametrization and the density of falling ice ρ_f. The treatment of cloud radiative properties also contains some highly uncertain parameters, such as the asymmetry parameter for ice clouds g_i and the factor ξ which reduces the optical depth to compensate for the treatment of clouds as plane-parallel. The sensitivity of the model simulation to some of these parameters will be examined in Part II.

(e) *Validation of the large-scale cloud fields*

A preliminary validation of the large-scale cloud-fields focused on July global-mean and zonal-mean results from a six-year run using the control version of the scheme. The results generally agreed well with observations, and showed a marked improvement in the modelled cloudiness and LWCF, as compared with a run using the standard Mark 2 version of the CSIRO. Deficiencies noted were similar to those which have been found in many other GCMs, in particular, insufficient cloud-cover in the subtropics (probably due to insufficient vertical resolution in the boundary layer), excessive SWCF in the tropics, and insufficient SWCF in the mid-latitude storm tracks.

A possible cause of the deficiencies in the SWCF is the coarse horizontal resolution of the model—at R21 it is difficult for the model to resolve the mid-latitude storm tracks adequately or the inter-tropical convergence zone (ITCZ). There is some evidence that the modelled liquid-water paths in the ITCZ are too large and that the peak values spread over too broad an area. This could explain the excessive SWCF in the tropics, but it is unclear at present to what extent the liquid-water paths can be blamed on inadequate resolution and to what extent the model's treatment of physical processes (such as convection) is at fault. Another possible cause of the deficiencies in the model's SWCF is the treatment of cloud radiative properties, which assumes that clouds are homogeneous and plane-parallel, except for the reduction of cloud optical depth by the factor ξ described in section 3. The factor ξ used here is based on large-eddy simulations by Kogan *et al.* (1995), but they considered only cases with a solar zenith angle of zero. There is both theoretical and observational evidence (Welch and Wielicki 1984; Loeb and Davies 1996) to suggest that the variation of cloud reflectivity with solar zenith-angle is not captured realistically by the plane-parallel approximation. These studies have suggested that the reflectivity of real clouds increases more strongly with increasing zenith-angle than does that of plane-parallel clouds. Moreover, the deficiencies in the model's SWCF noted here are qualitatively consistent with this finding, since the average solar zenith-angle in the mid-latitude storm tracks is larger than in the tropics. The modelled liquid-water paths over mid-latitude oceans of the northern hemisphere are larger than the observed (Fig. 15), also suggesting that the cloud radiative properties are a part of the problem, since it is the low-level liquid-water clouds which are the primary source of SWCF (although, as noted in section 6, the observed liquid-water paths are very uncertain at present). More detailed comparison of the model's large-scale cloudiness and cloud radiative forcing with observations is deferred until Part II.

ACKNOWLEDGEMENTS

This work has been performed as part of the author's PhD thesis; thanks are due to Dr Brian Ryan of CSIRO Division of Atmospheric Research and Professor David Karoly of Monash University for their advice and encouragement. The author is also pleased to acknowledge helpful conversations with a number of other scientists at CSIRO, in particular Drs Martin Platt, John McGregor, John Garratt and Hal Gordon. Thanks are due to Sarah Moss of the Meteorological Office who provided Fig. 5 in electronic form. This work contributes to the CSIRO Climate Change Research Program and is partly funded through Australia's National Greenhouse Research Program.

APPENDIX A

Physically based parametrization of mixed-phase clouds

Mixed-phase clouds generally consist mainly of supercooled water initially, because of the relative abundance of CCN compared to IFN. As the cloud evolves, ice crystals grow at the expense of liquid-water droplets, because the saturation vapour pressure is lower with respect to ice than with respect to water. This effect is commonly referred to as the Bergeron–Findeisen mechanism. The cloud model of RH83 included a parametrization for deposition on cloud ice in which the ice-crystal number concentration N_i (to which the calculation is sensitive) was assumed to follow the relation given by Fletcher (1962) for the concentration of IFN active at temperature T, viz.

$$N_i = N_{i0} \exp\{\eta(T_0 - T)\} \tag{A.1}$$

where $N_{i0} = 10^{-2}$ m^{-3} and $\eta = 0.6$ K^{-1}. However, observed ice-crystal number-concentrations can be several orders of magnitude greater than the IFN concentration due to ice-multiplication effects (RY88). This suggests that a reasonably rigorous approach might require the inclusion of ice-crystal number-concentration as a prognostic variable (e.g. Cotton *et al.* 1986) resulting in a substantial increase in computational complexity, while retaining a degree of uncertainty due to the currently incomplete understanding of the processes responsible for ice multiplication. An adaptation of the approach of RH83 would involve parametrizing the rate of growth of cloud ice (assumed to consist of monodispersed, hexagonal, plate-like crystals) by vapour deposition at the expense of supercooled water as

$$(\dot{q}_i)_{DE} = \frac{65.2 N_i^{1/2} q_i^{1/2} (e_{sl} - e_{si})}{\rho^{1/2}(A'' + B'')e_{si}}, \tag{A.2}$$

obtained by combining (A.17) and (A.18) of RH83 and assuming that the air is saturated with respect to liquid water. Here, A'' and B'' are temperature-dependent terms representing heat conduction and vapour diffusion respectively (defined in appendix B). Analytical integration of (A.2) with respect to time (treating q_i as the dependent variable) yields a version more suitable for implementation with large time-steps typical of GCMs. The rate of generation of cloud ice given by (A.2) varies as a function of temperature according to the square root of the prescribed ice-crystal concentration N_i, which increases with decreasing temperature, the term $1/(A'' + B'')$, which decreases with decreasing temperature and the *relative* difference between e_{sl} and e_{si} (or, equivalently, q_{sl} and q_{si}), which increases with decreasing temperature. The net effect is that the glaciation rate increases monotonically with decreasing temperature. The rate of glaciation also depends on the square root of the mixing ratio of cloud ice q_i, giving increased rates of glaciation in regions where ice is already present. It does not include a dependence of the glaciation rate on the observed

variation of ice-crystal habit with temperature and supersaturation (RY88) or on realistic values of the ice-crystal concentration. The resultant liquid fraction will also depend on the amount of liquid water present before the calculation (A.2) is performed, so that very moist clouds (e.g. in regions of strong uplift) will favour relatively high liquid fractions. Experiments with schemes based on (A.2) (not shown) yielded very low rates of deposition on cloud ice at temperatures above about $-15\,^{\circ}\mathrm{C}$, probably because of the underestimate of N_i entailed by the use of (A.1). In addition to these problems, it is uncertain how to organize the coexisting ice and liquid water within a grid box, and even how to specify the saturation mixing ratio q_s which is required by the condensation scheme.

It is also possible to calculate deposition on *falling* ice according to (30) when ice falls into a cloud containing supercooled liquid water, if the latter is assumed to be at liquid saturation. In this calculation, deposition on falling ice is treated in identically the same way as the sublimation of falling ice, except that $q_v > q_{si}$. This is an important mechanism in the 'seeder–feeder' process mentioned in section 3, in addition to the growth of ice particles by accretion (riming) of supercooled cloud droplets, parametrized in the scheme using (29). Calculation of deposition on falling ice in this manner has been omitted from the present scheme, as the assumption of saturation with respect to liquid water is incompatible with the assumptions used in the condensation scheme (see section 3).

Appendix B

Derivations and numerical details of the parametrizations of precipitation and related processes

The precipitation processes described in this appendix are applied in a split manner, i.e. sequentially. Where the numerical scheme used for each process is described, a superscript n denotes the value of a variable before application of that process, and a superscript $n+1$ denotes the updated value after application of the process.

Relation between the slope factor and rainfall rate

The local mixing ratio of rain $q_r^1 = q_r/f_r$ is given by

$$q_r^1 = \frac{1}{\rho}\int_0^\infty \rho_w \pi \frac{D_r^3}{6} N_r(D_r)\,\mathrm{d}D_r,$$

which implies, after substitution of (19), that

$$\lambda_r = \left(\frac{\pi \rho_w N_{0r}}{\rho q_r^1}\right)^{1/4}. \tag{B.1}$$

The mixing ratio of rain is not directly available, since it is not a prognostic variable of the scheme, but it can be estimated as

$$q_r^1 = \frac{R_r^1}{\rho \overline{V_r}}, \tag{B.2}$$

where $\overline{V_r}$ is the mass-weighted-mean fall-speed of rain, i.e.

$$\overline{V_r} = \frac{\int_0^\infty N_r(D_r) M(D_r) V_r(D_r)\,\mathrm{d}D_r}{\int_0^\infty N_r(D_r) M(D_r)\,\mathrm{d}D_r}.$$

This gives, after substitution of (17) and (18),

$$\overline{V_r} = 1.94 k_r \left(\frac{\rho_0}{\rho}\right)^{1/2} \lambda_r^{-1/2}. \tag{B.3}$$

The use of (B.2) and (B.3) in (B.1) gives

$$\lambda_r = \left(\frac{1.94\pi\rho_w N_{0r} k_r (\rho_0/\rho)^{1/2}}{R_r^l}\right)^{2/9}, \tag{B.4}$$

which gives (21) after evaluation of parameters.

Autoconversion of cloud liquid water

Analytical integration of (15) with respect to time yields

$$q_l(t) = C_l \left\{ \left(\frac{q_l(0)}{C_l}\right)^{-4/3} + \frac{4}{3} c_{AU} t \right\}^{-3/4}, \tag{B.5}$$

where $c_{AU} = 0.104 g E_{AU} \rho^{4/3} / (\mu (N_d \rho_w)^{1/3})$ is a constant at a given grid-point and time-step. This is implemented in the model as

$$q_l^{n+1} = C_l \max\left[q_{CR}, \left\{ \left(\frac{q_l^n}{C_l}\right)^{-4/3} + \frac{4}{3} c_{AU} \Delta t \right\}^{-3/4} \right], \tag{B.6}$$

with q_{CR} given by (16).

Collection of cloud liquid water by rain

The rate at which a raindrop of diameter D_r falling with speed $V_r(D_r)$ grows by collection of cloud liquid water is given by the continuous-collection equation (RY88)

$$\frac{dM(D_r)}{dt} = E_{CO} \frac{\pi}{4} D_r^2 V_r(D_r) \rho q_l \tag{B.7}$$

where $M(D_r)$ is the mass of a raindrop of diameter D_r and E_{CO} is the mean collection efficiency. Multiplication of (B.7) by (18), elimination of $V_r(D_r)$ using (17) and integration over all drop sizes gives the collection rate as

$$\rho(\dot{q}_l)_{CO} = -\frac{E_{CO}\pi k_r}{4} N_{0r} \left(\frac{\rho_0}{\rho}\right)^{1/2} \frac{\Gamma(3.5)}{\lambda_r^{3.5}} \rho q_l.$$

Elimination of λ_r using (B.4) and evaluation of parameters gives

$$(\dot{q}_l)_{CO} = -0.305 f_r E_{CO} \left(\frac{\rho_0}{\rho}\right)^{1/9} (R_r^l)^{7/9} q_l,$$

where the rainy fraction f_r has been included. Ignoring the weak dependence on ρ/ρ_0 and approximating $0.305(R_r^l)^{7/9}$ as $0.24(R_r^l)^{3/4}$ gives the computationally cheaper form (22) which yields similar results. The evaluation of q_l on the RHS of (22) is centred-in-time as $0.5(q_l^n + q_l^{n+1})$ to reduce time truncation errors; this gives

$$q_l^{n+1} = q_l^n \frac{1 - 0.5 c_{CO} \Delta t}{1 + 0.5 c_{CO} \Delta t},$$

where $c_{CO} = 0.24 f_r E_{CO} (R_r^l)^{3/4}$. This approach gives similar results to analytical integration of (22) but uses a little less computer time. This parametrization is also used for the collection of cloud liquid water by convective rain, and for the collection of cloud liquid water by raindrops generated within a grid box by autoconversion; in the latter case, the collection rate is multiplied by a factor of 0.5 because, in the mean, the raindrops are generated at the midpoint of the layer.

Evaporation of rain

The rate of evaporation of a raindrop of diameter D_r can be written as (RY88)

$$-\frac{dM(D_r)}{dt} = \frac{2\pi D_r (1 - S_l) F_r}{A' + B'}, \tag{B.8}$$

where $S_l = e/e_{sl}$ is the saturation ratio;

$$A' = \frac{L_V}{K_a T}\left(\frac{L_V}{R_v T} - 1\right)$$

and $B' = R_v T/\chi e_{sl}$ are terms representing heat conduction and vapour diffusion respectively. The inverse dependence of the diffusivity χ on pressure is taken into account. The ventilation factor is given by $F_r = 0.78 + 0.31 Sc^{1/3} Re^{1/2}$ (Beard and Pruppacher 1971), where $Sc = 0.6$ is the Schmidt number, and $Re = V_r(D_r) D_r \rho/\mu$ is the Reynolds number. Multiplication of (B.8) by (18), use of (17) for the fall speed and integration over all drop sizes gives

$$\rho(\dot{q}_v)_{EV} = \frac{2\pi N_{0r}(1 - S_l)}{A' + B'}\left\{\frac{0.78}{\lambda_r^2} + \frac{0.31 Sc^{1/3}}{\lambda_r^{2.75}}\left(\frac{k_r \rho}{\mu}\right)^{1/2} \Gamma(2.75)\left(\frac{\rho_0}{\rho}\right)^{1/4}\right\}. \tag{B.9}$$

This equation is similar to equation (A.12) of RH83, but using the relation (17) for the fall speed rather than their linear relation, and including the factor $Sc^{1/3}$ erroneously omitted from their expression. Since $Re \gg 1$ for raindrops, we can approximate $F_r = 0.31 Sc^{1/3} Re^{1/2}$ with little loss of accuracy, so that the first term in the square brackets in (B.9) drops out. With this simplification, use of the approximation $S_l = q_v/q_{sl}$, and use of (B.4) to eliminate λ_r, we obtain

$$(\dot{q}_v)_{EV} = \frac{1.04 N_{0r}^{7/18} Sc^{1/3} (q_{sl} - q_v)}{\rho^{1/2}(A' + B') k_r^{1/9} \mu^{1/2} \rho_w^{11/18} q_{sl}} (R_r^l)^{11/18},$$

where a factor $(\rho/\rho_0)^{1/18}$ has been ignored. After evaluation of parameters and inclusion of the rainy fraction f_r, (23) is obtained. Note that (23) can be made implicit (with respect to $q_{sl} - q_v$) by using the first-order terms in a Taylor series to obtain q_{sl}^{n+1} in terms of q_{sl}^n (Smith *et al.* 1995). If we write $(\dot{q}_v)_{EV} = c_{EV}(q_{sl} - q_v)$, this gives (after a little manipulation)

$$q_v^{n+1} = q_v^n + (c_{EV}^n \Delta t / b_{EV}^n)(q_{sl}^n - q_v^n),$$

where

$$b_{EV} = 1 + \gamma c_{EV} \Delta t \left\{1 + \frac{L_v}{c_p}\left(\frac{\partial q_s}{\partial T}\right)\right\}$$

and $\partial q_s/\partial T$ is obtained from the Clausius–Clapeyron equation. The parameter γ ($0 \leq \gamma \leq 1$) controls the amount of 'implicitness', so that, for example, $\gamma = 1$ gives

a fully implicit version whereas $\gamma = 0.5$ gives a time-centred version which has been adopted for the present scheme. The fully implicit scheme ensures that a grid box cannot become supersaturated through the evaporation of rain, whereas an extra line of code is required to enforce this condition if the time-centred scheme is used. Based on the vertical random-overlap assumption, the total evaporation $(q_v^{n+1} - q_v^n)$ is not allowed to exceed $(1 - C_l)R_r\Delta t/(\rho\Delta z)$.

Flux divergence of falling ice

Equation (25) is integrated analytically, treating R_f as a constant. This gives

$$q_i(t) = q_i(0)\exp\left(-\frac{\overline{V_f}t}{\Delta z}\right) + \frac{R_f}{\rho\overline{V_f}}\left\{1 - \exp\left(-\frac{\overline{V_f}t}{\Delta z}\right)\right\}$$

which is implemented in the model as

$$q_i^{n+1} = q_i^n \exp(-\alpha) + \frac{R_f\Delta t}{\rho\Delta z}\{1 - \exp(-\alpha)\}/\alpha, \tag{B.10}$$

where $\alpha = \overline{V_f}\Delta t/\Delta z$ is the Courant number*, and $R_f\Delta t/(\rho\Delta z)$ is the mixing ratio of ice which falls into the layer from above during the time-step. The parameter R_f is calculated as the average rate at which ice falls into the layer from above during the current time-step, less any sublimation, and is available since (B.10) has already been calculated for higher layers. Equation (B.10) shows clearly how the analytically integrated version determines the fraction of ice entering the layer from above which falls through, and the fraction of the ice present at the start of the time-step which falls out. The other schemes mentioned in the text (explicit, implicit, time-centred) can be expressed similarly.

Accretion of cloud liquid water by falling ice (snow)

The rate at which a (spherical) ice particle of diameter D_f falling with speed $V_f(D_f)$ grows by accretion of cloud liquid water is given by the continuous-collection equation

$$\frac{dM(D_f)}{dt} = E_{AC}\frac{\pi}{4}D_f^2 V_f(D_f)\rho q_l, \tag{B.11}$$

where $M(D_f)$ is the mass of a particle of diameter D_f and E_{AC} is the mean collection efficiency. Multiplication of (B.11) by (26) and integration over all particle sizes gives the accretion rate as

$$\rho(\dot{q}_l)_{AC} = -\frac{E_{AC}f_f\pi\overline{V_f}N_{0f}\Gamma(3)}{4\lambda_f^3}\rho q_l$$

if all ice is assumed to fall with the mass-weighted-mean fall-speed $\overline{V_f}$ and f_f is the snowy fraction of the grid box. Elimination of N_{0f} using (28), and substitution of the frozen-

* Here, the Courant number represents the number of model layers of depth Δz traversed during one time-step by a particle falling at $\overline{V_f}$.

precipitation rate $R_f = \rho q_f \overline{V_f}$, yields (29). As with the term for collection of cloud liquid water by rain, evaluation of q_l on the RHS of (29) is centred in time.

Sublimation of falling ice (snow)

The rate of sublimation of a falling ice particle of diameter D_f is given by (RY88):

$$-\frac{dM(D_f)}{dt} = \frac{4\pi \mathscr{C}_f (1 - S_i) F_f}{A'' + B''} \tag{B.12}$$

where $\mathscr{C}_f$ is the capacitance, $S_i = e/e_{si}$ is the saturation ratio and

$$A'' = \frac{L_S}{K_a T}\left(\frac{L_{SB}}{R_v T} - 1\right)$$

and $B'' = R_v T/\chi e_{si}$ are terms representing heat conduction and vapour diffusion respectively. The ventilation factor is $F_f = 0.65 + 0.44 Sc^{1/3} Re^{1/2}$ (Thorpe and Mason 1966), where $Re = V_f(D_f) D_f \rho/\mu$. Assuming that the particles are in the form of plate-like crystals for which $\mathscr{C}_f \approx D_f/\pi$, using the approximation $S_i = q_v/q_{si}$, multiplying (B.12) by (26) and integrating over all particle sizes, we obtain

$$(\dot{q}_v)_{SB} = f_f \frac{4(q_{si} - q_v) N_{0f}}{\rho(A'' + B'') q_{si}} \left\{ \frac{0.65}{\lambda_f^2} + \frac{0.493}{\lambda_f^{5/2}} \left(\frac{\overline{V_f}\rho}{\mu} \right)^{1/2} \right\} \tag{B.13}$$

if all ice particles are assumed to fall with the mass-weighted fall-speed $\overline{V_f}$ and sublimation occurs only in the snowy fraction f_f of the grid box. An alternative form of (B.13) in which the dependence on the snowfall rate is made explicit, is obtained by substitution of (28) to eliminate N_{0f} and use of the rate of frozen precipitation $R_f = \rho q_f \overline{V_f}$, which yields (30). This calculation is discretized in a time-centred manner, analogous to that used for the evaporation of rain.

Appendix C

Calculation of the fraction of a grid box into which precipitation falls

A number of the parametrizations described above require an estimate of the rainy or snowy fraction (i.e. the fraction of a grid box into which precipitation falls). Similar approaches are used for rain and falling ice (snow). In the following description, model levels are specified by superscripts, so that a superscript k denotes a quantity at the level under consideration and a superscript $k + 1$ denotes a quantity at the level immediately above.

Treatment of rain

For stratiform rainfall, the rainy fraction is calculated using the random-overlap assumption, as follows. The rainy fraction f_r^k in a grid box at level k is calculated as the sum of

- the fraction f_{rc}^k of the grid box into which rain falls from a cloud at level $k + 1$, and
- the fraction f_{ro}^k of the grid box into which rain falls from clear sky at level $k + 1$.

Rain which falls from a cloud at level $k + 1$ either originates in that cloud (by autoconversion) or at a higher level (by collection by stratiform or convective rain). Rain which

originates at level $k+1$ is assumed to fall from the entire (liquid water) cloud, so that $f_{rc}^k = C_l^{k+1}$ if autoconversion occurs at level $k+1$. Rain which forms at level $k+1$ from collection by rain falling from above is assumed to fall from a fraction of the cloud equal to the rainy fraction f_r^{k+1}, so that $f_{rc}^k = C_l^{k+1} f_r^{k+1}$ if autoconversion does not occur at level $k+1$. For simplicity, the scheme sets $f_{ro}^k = (1 - C_l^{k+1}) f_r^{k+1}$, unless all rain entering the clear portion of the grid box at level $k+1$ was found to evaporate, in which case $f_{ro}^k = 0$.

Since collection of cloud liquid water by convective precipitation is included in the scheme, an estimate of the rainy fraction for convective precipitation is also required. This is assumed to equal the randomly-overlapped convective-cloud cover above level k, calculated according to (10).

Treatment of falling ice

The fraction of a grid box into which ice falls is calculated in a manner similar to that described above for stratiform rain. The snowy fraction f_f^k in a grid box at level k is calculated as the sum of

- the fraction f_{fc}^k of the grid box into which ice falls from a cloud at level $k+1$, and
- the fraction f_{fo}^k of the grid box into which ice falls from clear sky at level $k+1$.

The first quantity is assumed to equal the ice cloud fraction at level $k+1$, i.e. $f_{fc}^k = C_i^{k+1}$. The second quantity comes from ice which falls through layer $k+1$ during the time-step; the scheme sets $f_{fo}^k = (1 - C_i^{k+1}) f_f^{k+1}$, unless all ice entering the clear portion of the grid box at level $k+1$ is found to evaporate, in which case $f_{fo}^k = 0$.

APPENDIX D

List of symbols

Symbol	Description	Value	Units
A'	Term representing heat conduction in evaporation equation		$\mathrm{m\,s\,kg^{-1}}$
A''	Term representing heat conduction in sublimation equation		$\mathrm{m\,s\,kg^{-1}}$
a_{CV}	Tunable parameter in convective cloudiness parametrization	0.2	
a_L	Factor accounting for latent heating in cloud		
B'	Term representing vapour diffusion in evaporation equation		$\mathrm{m\,s\,kg^{-1}}$
B''	Term representing vapour diffusion in sublimation equation		$\mathrm{m\,s\,kg^{-1}}$
b_{CV}	Tunable parameter in convective-cloudiness parametrization	0.07	
b_{EV}	Parameter in evaporation parametrization		
C	Stratiform cloud fraction		
$\mathscr{C}_f$	Capacitance of a falling ice particle		F
C_{CV}	Convective cloud fraction		
$\widetilde{C_{CV}}$	Total convective-cloud cover in a model column		
C_i	Stratiform ice-cloud fraction		
C_l	Stratiform liquid-water cloud fraction		
c_A	Tunable parameter in precipitation parametrization used by S90	1	$\mathrm{m^2 kg^{-1}}$
c_{AU}	Rate constant in autoconversion parametrization		$\mathrm{s^{-1}}$
c_{CO}	Rate constant in collection parametrization		$\mathrm{s^{-1}}$
c_{EV}	Rate constant in evaporation parametrization		$\mathrm{s^{-1}}$
c_p	Specific heat of dry air at constant pressure	1004.64	$\mathrm{J\,kg^{-1}K^{-1}}$

c_T	Tunable parameter in precipitation parametrization used by S90	10^{-4}	s^{-1}
c_W	Tunable parameter in precipitation parametrization used by S90	8×10^{-4}	kg kg^{-1}
D_r	Diameter of a raindrop		m
D_f	Diameter of a falling ice particle		m
E_{AU}	Autoconversion collection efficiency	0.55	
E_{CO}	Rain/cloud-liquid-water collection efficiency	0.7	
E_{AC}	Falling-ice/cloud-liquid-water collection efficiency	0.7	
e	Water-vapour pressure		Pa
e_{si}	Saturation vapour pressure with respect to ice		Pa
e_{sl}	Saturation vapour pressure with respect to liquid water		Pa
F_f	Ventilation factor for falling ice-particles		
F_r	Ventilation factor for raindrops		
$f(q)$	PDF for sub-grid distribution of total-water mixing ratio		
f_r	Rainy fraction of grid box		
f_{rc}	Rainy fraction resulting from rain falling from cloud at the level above		
f_{ro}	Rainy fraction resulting from rain falling from clear sky at the level above		
f_f	Snowy fraction of grid box		
f_{fc}	Snowy fraction resulting from ice falling from cloud at the level above		
f_{fo}	Snowy fraction resulting from ice falling from clear sky at the level above		
g	Acceleration under gravity	9.806	m s^{-2}
$\mathcal{G}_i$	Asymmetry parameter for ice clouds	0.8	
$H()$	Heaviside unit step function		
$\mathcal{H}$	Cloud optical depth diffusivity factor	1.6 or 1.8	
K_a	Thermal conductivity of air	2.40×10^{-2}	J $m^{-1}s^{-1}K^{-1}$
k_r	Constant in raindrop fall-speed relation	141.4	$m^{1/2}s^{-1}$
L	Latent heat (either L_V or $L_V + L_S$)		J kg^{-1}
L_S	Latent heat of sublimation of water	2.834×10^6	J kg^{-1}
L_V	Latent heat of vaporization of water	2.501×10^6	J kg^{-1}
$M(D_r)$	Mass of a raindrop of diameter D_r		kg
$M(D_f)$	Mass of a falling ice particle of diameter D_f		kg
N_{0f}	Intercept parameter in size distribution of falling ice particles		m^{-4}
N_{0r}	Intercept parameter in size distribution of raindrops	8×10^6	m^{-4}
N_{CV}	Number of convectively active levels		
N_d	Cloud-droplet concentration	1×10^8 (ocean) 5×10^8 (land)	m^{-3} m^{-3}
$N_f(D_f)dD_f$	Number of falling ice particles with diameters between D_f and $D_f + dD_f$		m^{-3}
$N_i(T)$	Ice-crystal concentration at temperature T		m^{-3}
N_{i0}	Ice-crystal concentration at temperature T_0	10^{-2}	m^{-3}
$N_r(D_r)dD_r$	Number of raindrops with diameters between D_r and $D_r + dD_r$		m^{-3}
P	Rate at which precipitation enters a layer from above		kg $m^{-2}s^{-1}$
p	Air pressure		Pa

p_*	Surface air pressure		Pa
Q_c	Generalized cloud-water mixing ratio		kg kg^{-1}
q	Total-water mixing ratio at a point within a grid box		kg kg^{-1}
q_c	Cloud-water mixing ratio		kg kg^{-1}
q_{CR}	Critical cloud-liquid-water mixing ratio		kg kg^{-1}
q_f	Mixing ratio of falling ice		kg kg^{-1}
q_i	Cloud-ice mixing ratio		kg kg^{-1}
$(\dot{q}_i)_{AV}$	Rate of change of q_i because of advection		kg kg^{-1}s^{-1}
$(\dot{q}_i)_{C/E}$	Rate of change of q_i because of formation or dissipation of stratiform cloud		kg kg^{-1}s^{-1}
$(\dot{q}_i)_{CV}$	Rate of change of q_i because of convection		kg kg^{-1}s^{-1}
$(\dot{q}_i)_{DE}$	Rate of change of q_i because of vapour deposition		kg kg^{-1}s^{-1}
$(\dot{q}_i)_{F/M}$	Rate of change of q_i because of freezing or melting		kg kg^{-1}s^{-1}
$(\dot{q}_i)_P$	Rate of change of q_i because of formation of precipitation		kg kg^{-1}s^{-1}
$(\dot{q}_i)_{TM}$	Rate of change of q_i because of turbulent mixing		kg kg^{-1}s^{-1}
q_l	Cloud liquid water mixing ratio		kg kg^{-1}
$(\dot{q}_l)_{AC}$	Rate of change of q_l because of accretion by falling ice		kg kg^{-1}s^{-1}
$(\dot{q}_l)_{AU}$	Rate of change of q_l because of autoconversion		kg kg^{-1}s^{-1}
$(\dot{q}_l)_{AV}$	Rate of change of q_l because of advection		kg kg^{-1}s^{-1}
$(\dot{q}_l)_{C/E}$	Rate of change of q_l because of formation or dissipation of stratiform cloud		kg kg^{-1}s^{-1}
$(\dot{q}_l)_{CO}$	Rate of change of q_l because of collection by rain		kg kg^{-1}s^{-1}
$(\dot{q}_l)_{CV}$	Rate of change of q_l because of convection		kg kg^{-1}s^{-1}
$(\dot{q}_l)_{F/M}$	Rate of change of q_l because of freezing or melting		kg kg^{-1}s^{-1}
$(\dot{q}_l)_P$	Rate of change of q_l because of formation of precipitation		kg kg^{-1}s^{-1}
$(\dot{q}_l)_{TM}$	Rate of change of q_l because of turbulent mixing		kg kg^{-1}s^{-1}
q_r	Mixing ratio of rain		kg kg^{-1}
q_s	Saturation mixing ratio		kg kg^{-1}
q_{si}	Saturation mixing ratio with respect to ice		kg kg^{-1}
q_{sl}	Saturation mixing ratio with respect to liquid water		kg kg^{-1}
q_t	Total-water mixing ratio		kg kg^{-1}
q_v	Water-vapour mixing ratio		kg kg^{-1}
$(\dot{q}_v)_{EV}$	Rate of change of q_v because of evaporation of rain		kg kg^{-1}s^{-1}
$(\dot{q}_v)_{SB}$	Rate of change of q_v because of sublimation of snow		kg kg^{-1}s^{-1}
R_{CV}	Convective rainfall rate at cloud base		mm d^{-1}
R_f	Frozen precipitation rate		kg m^{-2}s^{-1}
R_r	Rainfall rate		kg m^{-2}s^{-1}
R_v	Specific gas constant for water vapour	461	J kg^{-1}K^{-1}
RH_{CR}	Critical relative humidity for cloud formation	0.85 (ocean) 0.8 (land)	
r_{CR}	Critical cloud-droplet radius	9×10^{-6}	m
r_e	Effective radius		m
S_i	Saturation ratio with respect to ice		
S_l	Saturation ratio with respect to liquid water		
T	Air temperature		K
T_0	Melting point of ice	273.15	K
T_L	Liquid-frozen water temperature		K
t	Time		s
$V_f(D_f)$	Fall speed for an ice particle of diameter D_f		m s^{-1}

$\overline{V_f}$	Mass-weighted fall speed for ice particles		$m\ s^{-1}$
$V_r(D_r)$	Fall speed for a raindrop of diameter D_r		$m\ s^{-1}$
$\overline{V_r}$	Mass-weighted fall-speed for rain		$m\ s^{-1}$
W_i	Ice water content		$kg\ m^{-3}$
x	Any non-negative real number		
α	Courant number		
β_{ext}	Cloud visible volume extinction coefficient		m^{-1}
$\Gamma()$	Gamma function		
γ	Parameter in evaporation parametrization		
Δq	Half-width of total-water probability distribution function		$kg\ kg^{-1}$
Δt	Time-step		s
Δz	Model layer depth		m
δ_v	Cloud visible optical depth		
δ_a	Cloud infrared optical depth		
ϵ	Cloud emissivity		
η	Parameter in ice-crystal concentration parametrization	0.6	K^{-1}
λ_f	Slope factor in size distribution of falling ice particles		m^{-1}
λ_r	Slope factor in size distribution of raindrops		m^{-1}
μ	Dynamic viscosity of air	1.717×10^{-5}	$kg\ m^{-1}s^{-1}$
ξ	Scale factor for cloud optical depth		
ρ	Air density		$kg\ m^{-3}$
ρ_f	Bulk density of falling ice particles	100	$kg\ m^{-3}$
ρ_i	Density of ice	917	$kg\ m^{-3}$
ρ_w	Density of water	1000	$kg\ m^{-3}$
σ	Model vertical coordinate (p/p_*)		
σ_s	Standard deviation of the sub-grid fluctuations of Q_c		$kg\ kg^{-1}$
χ	Diffusivity of water vapour in air at 1000 hPa	2.21×10^{-5}	$m^2\ s^{-1}$

Superscripts

k	Denotes a quantity evaluated at model level k
l	Denotes the local value of a quantity (as distinct from the grid-box-mean value)
n	Denotes a quantity evaluated at time-step n.

REFERENCES

Arakawa, A 1972 Design of the UCLA general circulation model. Numerical simulation of weather and climate. Tech. Report No. 7, Dept. Meteor., Univ. California Los Angeles, USA

Beard, K. V. and Pruppacher, H. R. 1971 A wind tunnel investigation of the rate of evaporation of small water droplets falling at terminal velocity in air. *J. Atmos. Sci.*, **28,** 1455–1464

Bermejo, R. and Staniforth, A. 1992 The conversion of semi-Lagrangian advection schemes to quasi-monotone schemes. *Mon. Weather Rev.*, **120,** 2622–2632

Berry, E. X. and Reinhardt, R. L. 1974a An analysis of cloud drop growth by collection: Part I. Double distributions. *J. Atmos. Sci.*, **31,** 1814–1824

1974b An analysis of cloud drop growth by collection: Part II. Single initial distributions. *J. Atmos. Sci.*, **31,** 1825–1831

Boucher, O., Le Treut, H. and Baker, M. B. 1995 Precipitation and radiation modelling in a GCM: Introduction of cloud microphysical processes. *J. Geophys. Res.*, **100,** 16 395–16 414

Bower, K. N., Moss, S. J., Johnson, D. W., Choularton, T. W., Latham, J., Brown, P. R. A. and Cardwell, J. 1996 A parametrization of the ice water content observed in frontal and convective clouds. *Q. J. R. Meteorol. Soc.*, **122,** 1815–1844

Cahalan, R. F., Ridgeway, W., Wiscombe, W. J. and Bell, T. L. 1994 The albedo of fractal stratocumulus clouds. *J. Atmos. Sci.*, **51,** 2434–2455

Cess, R. D., Potter, G. L., Blanchett, J. P., Boer, G. J., Del Genio, A. D., Déqué, M., Dymnikov, V., Galin, V., Gates, W. L., Ghan, S. J., Kiehl, J. T., Lacis, A. A., Le Treut, H., Li, Z.-X., Liang, X.-Z., McAvaney, B. J., Meleshko, V. P., Mitchell, J. F. B., Morcrette, J.-J., Randall, D. A., Rikus, L., Roeckner, E., Royer, J. F., Schlese, U., Sheinin, D. A., Slingo, A., Sokolov, A. P., Taylor, K. E., Washington, W. M., Wetherald, R. T., Yagai, I. and Zhang, M.-H. 1990 Intercomparison and interpretation of climate feedback processes in 19 atmospheric general circulation models. *J. Geophys. Res.*, **95,** 16 601–16 615

Cess, R. D., Potter, G. L., Gates, W. L., Morcrette, J.-J. and Corsetti, L. 1992 Comparison of general circulation models to earth radiation budget experiment data: Computation of clear sky fluxes. *J. Geophys. Res.*, **97,** 20 421–20 426

Clough, S. A. and Franks, R. A. A. 1991 The evaporation of frontal and other stratiform precipitation. *Q. J. R. Meteorol. Soc.*, **117,** 1057–1080

Cotton, W. R., Stephens, M. A., Nehrkorn, T. and Tripoli, G. J. 1982 The Colorado State University three-dimensional cloud/mesoscale model—1982. Part II: An ice phase parameterization. *J. Rech. Atmos.*, **16,** 295–320

Cotton, W. R., Tripoli, G. J., Rauber, P. M. and Mulvihill, E. A. 1986 Numerical simulation of the effects of varying ice crystal nucleation rates and aggregation processes on orographic snowfall. *J. Climate Appl. Meteorol.*, **25,** 1658–1680

Ek, M. and Mahrt, L. 1991 A formulation for boundary layer cloud cover. *Ann. Geophysicae*, **9,** 716–724

Flato, G. M. and Hibler, W. III 1990 On a simple sea ice dynamics model for climate studies. *Adv. Geophys.*, **14,** 72–77

Fletcher, N. H. 1962 *The physics of rainclouds.* Cambridge University Press

Fowler, L. D., Randall, D. A. and Rutledge, S. A. 1996 Liquid and ice cloud microphysics in the CSU general circulation model. Part I: Model description and simulated microphysical processes. *J. Climate*, **9,** 489–529

Francis, P. N., Jones, A., Saunders, R. W., Shine, K. P., Slingo, A. and Sun, Z. 1994 An observational and theoretical study of the radiative properties of cirrus: Some results from ICE'89. *Q. J. R. Meteorol. Soc.*, **120,** 809–848

Gayet, J.-F., Giraud, V., Delannoy, A. and Larsen, H. 1993 'Description of the French microphysical data bank: Application to global change'. Pp. 188–193 in Proceedings of WMO workshop on cloud microphysics and applications to global change, 10–14 August 1992, Toronto, Canada. WMO/TD-no. 537. World Meteorological Organization

Geleyn, J. 1987 'Use of a modified Richardson number for parameterizing the effect of shallow convection'. Pp. 141–149 in Short- and Medium-Range Weather Prediction. Collection of Papers Presented at the WMO/IUGG NWP Symposium, Tokyo, 4–8 August 1986. Meteorological Society of Japan

Ghan, S. J. and Easter, R. C. 1992 Computationally efficient approximations to stratiform cloud microphysics parameterization. *Mon. Weather Rev.*, **120,** 1572–1582

Gordon, H. B. 1981 A flux formulation of the spectral atmospheric equations suitable for use in long term climate modeling. *Mon. Weather Rev.*, **109,** 56–64

Greenwald, T. J., Stephens, G. L., Vonder Haar, T. H. and Jackson, D. L.	1993	A physical retrieval of cloud liquid water over the global oceans using special sensor microwave/imager (SSM/I) observations. *J. Geophys. Res.*, **98,** 18 471–18 489
Gregory, D.	1995	A consistent treatment of the evaporation of rain and snow for use in large-scale models. *Mon. Weather Rev.*, **123,** 2716–2732
Gunn, R. and Kinzer, G. D.	1949	The terminal velocity of fall for water drops in stagnant air. *J. Meteorol.*, **6,** 243–248
Hack, J. J., Boville, B. A., Briegleb, B. P., Kiehl, J. T., Rasch, P. J. and Williamson, D. L.	1993	'Description of the NCAR Community Climate Model (CCM2)'. Tech. Note TN-382+STR, NCAR, Boulder, CO, USA
Harshvardhan and Randall, D. A.	1985	Comments on 'The parameterization of radiation for numerical weather prediction and climate models'. *Mon. Weather Rev.*, **113,** 1832–1835
Heymsfield, A. J.	1977	Precipitation development in stratiform ice clouds: a microphysical and dynamical study. *J. Atmos. Sci.*, **34,** 367–381
	1993	'Microphysical structures of stratiform and cirrus clouds'. Pp. 97–121 in *Aerosol-Cloud-Climate Interactions*, P. V. Hobbs Ed., Academic Press
Heymsfield, A. J. and Miloshevich, L. M.	1995	Relative humdity and temperature influences on cirrus formation and evolution: observations from wave clouds and FIRE II. *J. Atmos. Sci.*, **52,** 4302–4326
Holtslag, A. A. M. and Boville, B. A.	1993	Local versus non-local boundary layer diffusion in a global climate model. *J. Climate*, **6,** 1825–1842
Jakob, C. and Morcrette, J.-J.	1995	'Sensitivity of the ECMWF model to the treatment of the ice phase'. Pp. 37–46 in Proceedings of Workshop on cloud microphysics parameterizations in global atmospheric circulation models. WMO/TD no. 713. World Meteorological Organization
Jones, A., Roberts, D.L. and Slingo, A.	1994	A climate model study of indirect anthropogenic sulphate aerosols. *Nature*, **370,** 450–453
Katzfey, J. J.	1994	'Investigations of cumulus parameterizations for an Australian coastal low'. Pp. 129–134 in Parameterisation of physical processes: papers presented at the fifth BMRC Modelling Workshop, November 1993, J. D. Jasper, and P. J. Meighen Eds., BMRC, GPO Box 1289K, Melbourne, 3001, Australia
Kessler, E.	1969	'On the distribution and continuity of water substance in atmospheric circulation', Vol. 10 no. 32 of *Meteorol. Mono.* Amer. Meteorol. Soc., Boston, USA
Kogan, Z. N., Lilly, D. K., Kogan, Y. L. and Filyushkin, V.	1995	Evaluation of radiative parameterizations using an explicit cloud microphysical model. *Atmos. Res.*, **35,** 157–172
Kowalczyk, E. A., Garratt, J. R. and Krummel, P. B.	1991	'A soil-canopy scheme for use in a numerical model of the atmosphere—1D stand-alone model'. Tech. Paper No. 23, CSIRO Div. Atmos. Res., PMB1, Aspendale, Vic., 3195, Australia
Kristjánsson, J. E.	1994	Tests of a new cloud treatment in an atmospheric general circulation model. *Physica D*, **77,** 23–32
Lacis, A. A. and Hansen, J. E.	1974	A parameterization for the absorption of solar radiation in the Earth's atmosphere. *J. Atmos. Sci.*, **31,** 118–133
Le Treut, H. and Li, Z.-X.	1988	Using Meteosat data to validate a prognostic cloud generation scheme. *Atmos. Res.*, **21,** 273–292
Le Treut, H., Li, Z.-X. and Forichan, M.	1994	Sensitivity of the LMD general circulation model to greenhouse forcing associated with two different cloud water parameterizations. *J. Climate*, **7,** 1827–1841
Lin, Y.-L., Farley, R. D. and Orville, H. D.	1983	Bulk parameterization of the snow field in a cloud model. *J. Climate Appl. Meteorol.*, **22,** 1065–1092
Locatelli, J. D. and Hobbs, P. V.	1974	Fallspeeds and masses of solid precipitation particles. *J. Geophys. Res.*, **79,** 2185–2197
Loeb, N. G. and Davies, R.	1996	Observational evidence of plane parallel model biases: apparent dependence of cloud optical depth on solar zenith angle. *J. Geophys. Res.*, **101,** 1621–1634
Louis, J.-F.	1979	A parametric model of vertical eddy fluxes in the atmosphere. *Boundary-Layer Meteorol.*, **17,** 187–202

Manton, M. J. and Cotton, W. R. 1977 'Formulation of approximate equations for modeling moist deep convection on the mesoscale'. Atmos. Sci. Paper No. 266, Dept. Atmos. Sci., Colorado State University, Fort Collins, CO, USA

Marshall, K. S. and Palmer, W. M. 1948 The distribution of raindrops with size. *J. Meteorol.*, **5,** 165–166

Martin, G. M., Johnson, D. W. and Spice, A. 1994 The measurement and parameterization of effective radius of droplets in warm stratocumulus clouds. *J. Atmos. Sci.*, **51,** 1823–1842

Mason, B. J. 1971 *The physics of clouds* (2nd edition). Clarendon Press, Oxford

1975 *Clouds, rain and rainmaking* (2nd edition). Cambridge University Press

Mazin, I. P. 1994 On the climatology and physical structure of clouds. *Atmospheric and Oceanic Physics*, **30,** 318–324

McGregor, J. L., Gordon, H. B., Watterson, I. G., Dix, M. R. and Rotstayn, L. D. 1993 'The CSIRO 9-level atmospheric general circulation model'. Tech. Paper No. 26, CSIRO Div. Atmos. Res., PMB1, Aspendale, Vic., 3195, Australia

McGregor, J. L. 1993 Economical determination of departure points for semi-Lagrangian models. *Mon. Weather Rev.*, **121,** 221–230

Mitchell, J. F. B., Senior, C. A. and Ingram, W. J. 1989 CO_2 and climate: A missing feedback? *Nature*, **341,** 132–134

Ose, T. 1993 An examination of the effects of explicit cloud water in the UCLA GCM. *J. Meteorol. Soc. Japan*, **71,** 93–109

Pitter, R. L. and Pruppacher, H. R. 1974 A numerical simulation of collision efficiencies of simple ice plates colliding with supercooled water drops. *J. Atmos. Sci.*, **31,** 551–557

Platt, C. M. R. 1994 'Parameterization of cloud-radiation interactions from observations'. Pp. 153–158 in Parametrisation of physical processes: Papers presented at the fifth BMRC Modelling Workshop, November 1993, J. D. Jasper, and P. J. Meighen Eds., BMRC, GPO Box 1289K, Melbourne, 3001, Australia

1997 A parametrization of the visible extinction coefficient of ice clouds in terms of ice content. *J. Atmos. Sci.*, **53.** In press

Platt, C. M. R. and Stephens, G. L. 1980 The interpretation of remotely sensed high cloud emittances. *J. Atmos. Sci.*, **37,** 2314–2322

Randall, D. A. 1989 Cloud parameterization for climate modelling: Status and prospects. *Atmos. Res.*, **23,** 345–361

Rangno, A. L. and Hobbs, P. V. 1994 Ice particle concentrations and precipitation development in small continental cumuliform clouds. *Q. J. R. Meteorol. Soc.*, **120,** 573–601

Ricard, J. L. and Royer, J. F. 1993 A statistical cloud scheme for use in an AGCM. *Ann. Geophysicae*, **11,** 1095–1115

Roeckner, E., Arpe, K., Bengtsson, L., Brinkop, S., Dümenil, L., Esch, M., Kirk, E., Lunkeit, F., Ponater, M., Rockel, B., Sausen, R., Schlese, U., Schubert, S. and Windelband, M. 1992 'Simulation of the present-day climate with the ECHAM model: Impact of model physics and resolution'. Report No. 93, Max-Planck-Institut für Meteorologie, Hamburg, Germany

Rogers, R. R. and Yau, M. K. 1988 *A short course in cloud physics* (3rd edition). Pergamon Press, Oxford

Rossow, W. B., Walker, A. W., Beuschel, D. E. and Roiter, M. D. 1996 'International satellite cloud climatology project (ISCCP) documentation of new cloud datasets'. WMO/TD-No. 737, World Meteorological Organization

Rutledge, S. A. and Hobbs, P. V. 1983 The mesoscale and microscale structure and organization of clouds and precipitation in midlatitude cyclones. VIII: A model for the "seeder-feeder" process in warm-frontal rainbands. *J. Atmos. Sci.*, **40,** 1185–1206

Ryan, B. F., Wishart, E. R. and Shaw, D. E. 1976 The growth rates and densities of ice crystals between $-3\,^{\circ}C$ and $-21\,^{\circ}C$. *J. Atmos. Sci.*, **33,** 842–850

Ryan, B. F. 1996 On the global variation of precipitating layer clouds. *Bull. Amer. Meteorol. Soc.*, **77,** 53–70

Sauvageot, H. and Lacaux, J.-P. 1995 The shape of averaged drop size distributions. *J. Atmos. Sci.*, **52,** 1070–1083

Schwarzkopf, M. D. and Fels, S. B. 1991 The simplified exchange method revisited: An accurate, rapid method for computation of infrared cooling rates and fluxes. *J. Geophys. Res.*, **96,** 9075–9096

Semtner, A. J. Jr. 1976 A model for the thermodynamic growth of sea ice in numerical investigations of climate. *J. Phys. Oceanogr.*, **6,** 379–389

Senior, C. A. and Mitchell, J. F. B. 1993 Carbon dioxide and climate: The impact of cloud parameterization. *J. Climate*, **6,** 393–418

Simmons, A. J. and Jiabin, C. 1991 The calculation of geopotential and the pressure gradient in the ECMWF atmospheric model: Influence on the simulation of the polar atmosphere and on temperature analyses. *Q. J. R. Meteorol. Soc.*, **117,** 29–58

Simmons, A. J., Burridge, D. M., Jarraud, M., Girard, C. and Wergen, W. 1989 The ECMWF medium-range prediction models. Development of the numerical formulations and the impact of increased resolution. *Meteorol. Atmos. Phys.*, **40,** 28–60

Slingo, A. 1989 A GCM parameterization for the shortwave radiative properties of water clouds. *J. Atmos. Sci.*, **46,** 1419–1427

Slingo J. M. 1987 The development and verification of a cloud prediction scheme for the ECMWF model. *Q. J. R. Meteorol. Soc.*, **113,** 899–927

Smith, R. N. B. 1990 A scheme for predicting layer clouds and their water content in a general circulation model. *Q. J. R. Meteorol. Soc.*, **116,** 435–460

1993 'Experience and developments with the layer cloud and boundary layer mixing schemes in the UK Meteorological Office Unified Model'. Pp. 319–339 in Proceedings of a workshop held at ECMWF on parametrization of the cloud topped boundary layer, 8–11 June 1993, Reading. ECMWF

Smith, R., Gregory, D., Mithcell, J. and Bushell, A. 1995 'Large-scale precipitation'. Documentation Paper No. 26, Unified Model, Available from the Unified Model Librarian, NWP-Division, Meteorological Office, Bracknell, Berkshire, RG12 2SX

Stephens, G. L., Tsay, S.-C., Stackhouse, J. P. W. and Flatau, P. J. 1990 The relevance of the microphysical and radiative properties of cirrus clouds to climate and climatic feedback. *J. Atmos. Sci.*, **47,** 1742–1753

Sun, Z. and Shine, K. P. 1994 Studies of the radiative properties of ice and mixed-phase clouds. *Q. J. R. Meteorol. Soc.*, **120,** 111–138

Sundqvist, H. 1978 A parameterization scheme for non-convective condensation including prediction of cloud water content. *Q. J. R. Meteorol. Soc.*, **104,** 677–690

Sundqvist, H., Berge, E. and Kristjánsson, J. E. 1989 Condensation and cloud parameterization studies with a mesoscale numerical weather prediction model. *Mon. Weather Rev.*, **117,**, 1641–1657

Taylor, K. E. and Penner, J. E. 1994 Response of the climate system to atmospheric aerosols and greenhouse gases. *Nature*, **369,** 734–737

Thorpe, A. D. and Mason, B. J. 1966 The evaporation of ice spheres and ice crystals. *Brit. J. Appl. Phys.*, **17,** 541–551

Tian, L. and Curry, J. A. 1989 Cloud overlap statistics. *J. Geophys. Res.*, **94,** 9925–9935

Tiedtke, M. 1988 'Parameterization of cumulus convection in large-scale models'. Pp. 375–431 in *Physically Based Modelling and Simulation of Climate and Climatic Change—Part I*, M. Schlesinger Ed., Kluwer Academic Publishers

1993 Representation of clouds in large-scale models. *Mon. Weather Rev.*, **121,** 3040–3061

1996 An extension of cloud-radiation parameterization in the ECMWF model: the representation of subgrid-scale variations of optical depth. *Mon. Weather Rev.*, **124,** 745–750

Tripoli, G. J. and Cotton, W. R. 1980 A numerical investigation of several factors contributing to the observed variable intensity of deep convection over south Florida. *J. Appl. Meteorol.*, **19,** 1037–1063

Warren, S. G., Hahn, C. J., London, J., Chervin, R. M. and Jenne, R. L. 1986 'Global distribution of total cloud cover and cloud type amounts over land'. Tech. Note TN-273+STR, NCAR, Boulder, CO, USA

1988 'Global distribution of total cloud cover and cloud type amounts over the ocean'. Tech. Note TN-317+STR, NCAR, Boulder, CO, USA

Welch, R. M. and Wielicki, B. A. 1984 Stratocumulus cloud field reflected fluxes: the effect of cloud shape. *J. Atmos. Sci.*, **41,** 3085–3103

Weng, F. and Grody, N. C. 1994 Retrieval of cloud liquid water using the Special Sensor Microwave Imager (SSM/I). *J. Geophys. Res.*, **99**, 25 535–25 551